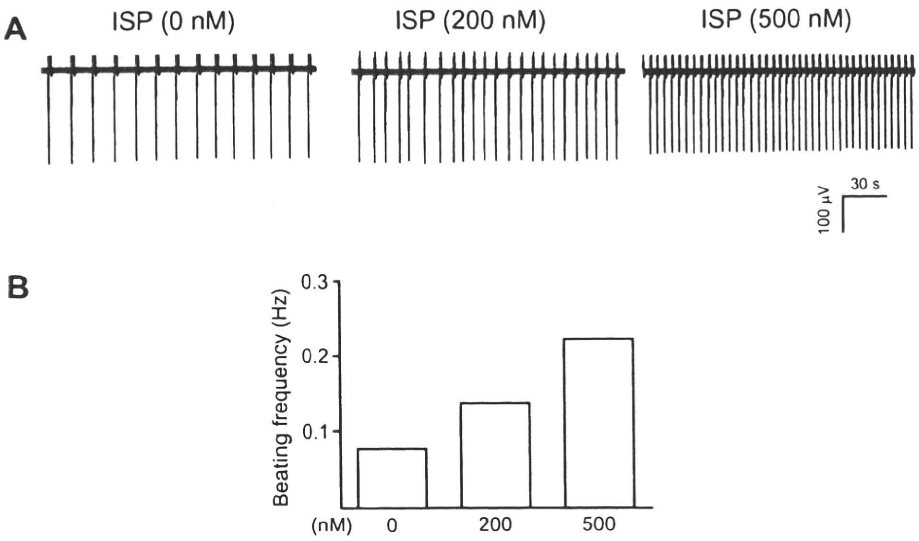

Fig. 3. Effect of isoproterenol on FP frequency. (A) Representative FP traces taken before and after the application of isoproterenol (ISP). (B) The graph shows a summary of the changes in the beating frequency caused by ISP.

due to their high costs. Furthermore, using the current system, it is difficult to predict accurately the occurrence of lethal side-effects. Thus, an *in vitro* model for drug screening is required, to avoid the withdrawal of drugs that have been costly to develop. We established a novel *in vitro* drug screening model to evaluate drug-induced changes in the electrophysiological properties of hiPS-CMs. In the present study, we measured FP using the MEA system. Although FP does not allow the derivation of an absolute measure of the individual ion currents that contribute to the AP, our MEA system clearly reveals the FP waveform changes induced by several anti-arrhythmia drugs [13]. This indicates the potential for using a combination of the hiPS-CM and MEA systems for drug testing.

In the present study, cardiomyocytes were differentiated from hiPS cells that were reprogrammed by four transcription factors (Oct3/4, Sox2, Klf4, and c-Myc) derived from adult dermal fibroblasts. A recent study demonstrated that functional hiPS-CMs could be generated from newborn foreskin fibroblasts or fetal lung fibroblasts by transduction with different sets of transcription factors, including Oct3/4, Sox2, Nanog, and LIN28 [14]. These cells displayed the typical cardiac phenotypes, including the expression of cardiac-specific transcription factors and sarcomeric proteins, as well as the appropriate responses to anti-arrhythmia drugs and adrenergic stimulants. No major differences in structural and functional properties were observed for the hiPS-CMs derived from the two different hiPS cell lines. The universal functional properties of hiPS-CMs may facilitate the application of hiPS technology to preclinical drug development.

Although many genetic cardiac disorders, such as familial cardiomyopathy, arrhythmias, and congenital heart diseases, have been identified, their underlying genetic mechanisms are largely unknown. Therefore, it is necessary to clarify the development, pathogenesis, and physiologic characteristics of these intractable diseases. In this regard, hiPS cells may provide an adequate supply of customized patient-specific cells for genetic and functional analyses, thereby enhancing the potential for clinical applications. However, the concerns about iPS systems, which are related to low differentiation efficiency and tumor formation that is probably due to the transduction of oncogenic factors and integration of vector viruses, need to be resolved before they can be used for cell replacement therapy. Recently, several groups reported that iPS cell lines could be established without c-Myc or viral vectors [15–17], or without the use of genes [18]. These progressive technologies may allow the utilization of safer hiPS cell lines.

Sources of funding

This work was performed as a part of a research and development projects of the Industrial Science and Technology Program supported by the New Energy and Industrial Technology Development Organization (NEDO).

Disclosures

None.

Acknowledgments

We thank Michiko Abe and Maki Doi for secretary assistance.

References

[1] L. Carlsson, In vitro and in vivo models for testing arrhythmogenesis in drugs, J. Intern. Med. 259 (2006) 70–80.
[2] P.J. Kannankeril, D.M. Roden, Drug-induced long QT and torsade de pointes: recent advances, Curr. Opin. Cardiol. 22 (2007) 39–43.
[3] M.B. Thomsen, J. Matz, P.G. Volders, M.A. Vos, Assessing the proarrhythmic potential of drugs: current status of models and surrogate parameters of torsades de pointes arrhythmias, Pharmacol. Ther. 112 (2006) 150–170.
[4] J.C. Brimecombe, G.E. Kirsch, A.M. Brown, Test article concentrations in the hERG assay: losses through the perfusion, solubility and stability, J. Pharmacol. Toxicol. Methods 59 (2009) 29–34.
[5] K. Takahashi, K. Tanabe, M. Ohnuki, M. Narita, T. Ichisaka, K. Tomoda, S. Yamanaka, Induction of pluripotent stem cells from adult human fibroblasts by defined factors, Cell 131 (2007) 861–872.
[6] K. Takahashi, S. Yamanaka, Induction of pluripotent stem cells from mouse embryonic and adult fibroblast cultures by defined factors, Cell 126 (2006) 663–676.
[7] J. Yu, M.A. Vodyanik, K. Smuga-Otto, J. Antosiewicz-Bourget, J.L. Frane, S. Tian, J. Nie, G.A. Jonsdottir, V. Ruotti, R. Stewart, I.I. Slukvin, J.A. Thomson, Induced pluripotent stem cell lines derived from human somatic cells, Science 318 (2007) 1917–1920.
[8] J.T. Dimos, K.T. Rodolfa, K.K. Niakan, L.M. Weisenthal, H. Mitsumoto, W. Chung, G.F. Croft, G. Saphier, R. Leibel, R. Goland, H. Wichterle, C.E. Henderson, K. Eggan, Induced pluripotent stem cells generated from patients with ALS can be differentiated into motor neurons, Science 321 (2008) 1218–1221.

[9] A.D. Ebert, J. Yu, F.F. Rose Jr., V.B. Mattis, C.L. Lorson, J.A. Thomson, C.N. Svendsen, Induced pluripotent stem cells from a spinal muscular atrophy patient, Nature 457 (2009) 277–280.
[10] F. Soldner, D. Hockemeyer, C. Beard, Q. Gao, G.W. Bell, E.G. Cook, G. Hargus, A. Blak, O. Cooper, M. Mitalipova, O. Isacson, R. Jaenisch, Parkinson's disease patient-derived induced pluripotent stem cells free of viral reprogramming factors, Cell 136 (2009) 964–977.
[11] H. Suemori, K. Yasuchika, K. Hasegawa, T. Fujioka, N. Tsuneyoshi, N. Nakatsuji, Efficient establishment of human embryonic stem cell lines and long-term maintenance with stable karyotype by enzymatic bulk passage, Biochem. Biophys. Res. Commun. 345 (2006) 926–932.
[12] I. Suzuki, K. Yasuda, Detection of tetanus-induced effects in linearly lined-up micropatterned neuronal networks: application of a multi-electrode array chip combined with agarose microstructures, Biochem. Biophys. Res. Commun. 356 (2007) 470–475.
[13] M. Halbach, U. Egert, J. Hescheler, K. Banach, Estimation of action potential changes from field potential recordings in multicellular mouse cardiac myocyte cultures, Cell. Physiol. Biochem. 13 (2003) 271–284.
[14] J. Zhang, G.F. Wilson, A.G. Soerens, C.H. Koonce, J. Yu, S.P. Palecek, J.A. Thomson, T.J. Kamp, Functional cardiomyocytes derived from human induced pluripotent stem cells, Circ. Res. 104 (2009) e30–e41.
[15] M. Nakagawa, M. Koyanagi, K. Tanabe, K. Takahashi, T. Ichisaka, T. Aoi, K. Okita, Y. Mochiduki, N. Takizawa, S. Yamanaka, Generation of induced pluripotent stem cells without Myc from mouse and human fibroblasts, Nat. Biotechnol. 26 (2008) 101–106.
[16] K. Okita, M. Nakagawa, H. Hyenjong, T. Ichisaka, S. Yamanaka, Generation of mouse induced pluripotent stem cells without viral vectors, Science 322 (2008) 949–953.
[17] J. Yu, K. Hu, K. Smuga-Otto, S. Tian, R. Stewart, I.I. Slukvin, J.A. Thomson, Human induced pluripotent stem cells free of vector and transgene sequences, Science (2009) (Epub ahead of print).
[18] H. Zhou, S. Wu, JY. Joo, S. Zhu, DW. Han, T. Lin, S. Trauger, G. Bien, S. Yao, Y. Zhu, G. Siuzdak, HR. Schöler, L. Duan, S. Ding, Generation of induced pluripotent stem cells using recombinant proteins, Cell Stem Cell 4 (2009) 1–4.

FEBS Letters 583 (2009) 2157–2159

FEBS Letters

journal homepage: www.FEBSLetters.org

Hypothesis

Are the effects of α-glucosidase inhibitors on cardiovascular events related to elevated levels of hydrogen gas in the gastrointestinal tract?

Yoshihiko Suzuki [a], Motoaki Sano [c,*], Kentaro Hayashida [c], Ikuroh Ohsawa [a,b], Shigeo Ohta [a], Keiichi Fukuda [c]

[a] Department of Biochemistry and Cell Biology, Institute of Development and Aging Science, Graduate School of Medicine, Nippon Medical School, Kawasaki City 211-8533, Japan
[b] The Center of Molecular Hydrogen Medicine, Institute of Development and Aging Science, Graduate School of Medicine, Nippon Medical School, Kawasaki City 211-8533, Japan
[c] Department of Regenerative Medicine and Advanced Cardiac Therapeutics, Keio University School of Medicine, Tokyo 160-8582, Japan

ARTICLE INFO

Article history:
Received 20 April 2009
Revised 28 May 2009
Accepted 31 May 2009
Available online 6 June 2009

Edited by Quan Chen

Keywords:
α-Glucosidase inhibitors
Type 2 diabetes
Hydrogen gas
Antioxidant

ABSTRACT

The major side-effect of treatment with α-glucosidase inhibitors, flatulence, occurs when undigested carbohydrates are fermented by colonic bacteria, resulting in gas formation. We propose that the cardiovascular benefits of α-glucosidase inhibitors are partly attributable to their ability to neutralise oxidative stress via increased production of H_2 in the gastrointestinal tract. Acarbose, which is an α-glucosidase inhibitor, markedly increased H_2 production, with a weaker effect on methane production. Our hypothesis is based on our recent discovery that H_2 acts as a unique antioxidant, and that when inhaled or taken orally as H_2-dissolved water it ameliorates ischaemia–reperfusion injury and atherosclerosis development.

1. Introduction

A growing body of evidence supports the notion that postprandial hyperglycaemia plays an important role in the development of cardiovascular disease. Large epidemiological studies have shown that the serum glucose concentration 2 h after an oral glucose challenge is a powerful predictor of cardiovascular risk [1,2].

α-Glucosidase inhibitors are pharmacological agents that specifically reduce postprandial hyperglycaemia through retardation of disaccharide digestion, thereby reducing glucose absorption by the small intestine. The STOP-NIDDM trial demonstrated that the treatment of patients who had impaired glucose tolerance with the α-glucosidase inhibitor acarbose was associated with a 25% reduction in the risk of progression to diabetes, a 34% reduction in the risk of developing *de novo* hypertension, and a 49% risk reduction for cardiovascular events [3]. Furthermore, a meta-analysis of seven long-term studies suggested that acarbose reduced the risk of myocardial infarction for patients with type 2 diabetes [4]. Such risk reduction for coronary heart disease events in patients with type 2 diabetes was not observed by the improved glycaemic control achieved with intensified treatment with insulin and glibenclamid [5]. Inhibition of postprandial hyperglycaemia by α-glucosidase inhibitors alleviates cardiac ischaemia–reperfusion injury in mice [6]. These findings suggest that α-glucosidase inhibitors interfere with the development of macrovascular diseases through additional mechanisms distinct from the expected modulation of postprandial hyperglycaemia.

2. Molecular hydrogen (H_2) acts as a novel antioxidant

Clinical evidence and experimental results strongly implicate reactive oxygen species (ROS) as the leading etiologic agent of cardiovascular diseases, including hypertension, atherosclerosis, angina pectoris, myocardial infarction, and heart failure [7,8]. The mechanisms for ROS production are diverse, and include increases in the activities of NAD(P)H-oxidase, xanthione oxidase, cyclooxygenase, and lipoxygenase, as well as uncoupling of nitric oxide synthase, dysfunction of the mitochondrial respiratory chain, and decreased bioavailability of antioxidants, all of which contribute to increased oxidative stress. An increase in ROS production reduces the bioavailability of nitric oxide (NO), synergistically advancing the pathogenesis of cardiovascular disease, since NO plays important roles in the regulation of vascular tone, inhibition of platelet aggregation, and suppression of smooth muscle cell (SMC) proliferation. Increases in the renal levels of ROS raise the blood pressure by influencing afferent arteriolar tone, tubulo-glomerular feedback response, and sodium reabsorption [9]. Increases in vascular ROS promote endothelial dysfunction, increased

* Corresponding author. Address: Department of Regenerative Medicine and Advanced Cardiac Therapeutics, Keio University School of Medicine, 35 Shinanomachi Shinjuku-ku, Tokyo 160-8582, Japan. Fax: +81 3 5363 3875.
E-mail address: msano@sc.itc.keio.ac.jp (M. Sano).

0014-5793/$36.00
doi:10.1016/j.febslet.2009.05.052

contractility, monocyte invasion, VSMC proliferation, and increased deposition of extracellular matrix proteins, all of which contribute to the pathogenesis of hypertension, atherosclerosis, and plaque rupture. In the brain, increased production of ROS mediates hypertension by increasing sympathetic outflow. Various antioxidants have been tested for their abilities to reduce the risk of cardiovascular disease. However, these trials have not verified the importance of antioxidants in the prevention of cardiovascular disease [10]. These outcomes can be partially explained by the dual roles of ROS. Most of the detrimental effects of ROS are attributed to ·OH, which is the most reactive oxygen species. In comparison, O_2^{-}· and H_2O_2 have lower oxidative energies and, paradoxically, are implicated as crucial signalling components in the establishment of favourable tolerance to oxidative stress. Consequently, the inhibition of both these pathways (e.g., by antioxidants) can have a deleterious outcome.

Recently, we discovered that molecular hydrogen (H_2) acts as an antioxidant with the following interesting properties: (i) H_2 permeates cell membranes and can target the cellular organelles, including the mitochondria and nuclei; and (ii) H_2 specifically quenches detrimental ROS, such as ·OH and peroxynitrite ($ONOO^-$), while maintaining the metabolic oxidation–reduction reaction and other less-potent ROS, such as O_2^{-}·, H_2O_2 and nitric oxide (NO·) [11]. We showed that inhalation of H_2 gas, given at an incombustible level, limited the extent of myocardial infarction resulting from myocardial ischaemia–reperfusion injury, thereby preventing deleterious left ventricular remodelling in the rat [12]. Importantly, the inhaled H_2 gas was transported rapidly in the circulation and reached the 'at-risk' ischaemic myocardium before the coronary blood flow of the occluded infarct-related artery was re-established.

H_2 can also be administered orally in the form of H_2-dissolved water. Kajiyama et al. reported that supplementation with 900 ml/day (300 ml given three times a day) of H_2-dissolved water for 8 weeks reduced the levels of several biomarkers of oxidative stress, such as plasma oxidized low-density lipoprotein (LDL) cholesterol and urinary 8-isoprostanes, and improved glucose metabolism in patients with type 2 diabetes or impaired glucose tolerance [13]. Furthermore, supplementation with H_2-dissolved water normalized the oral glucose tolerance test in four out of six patients with impaired glucose tolerance. The reduction in the expression of biomarkers associated with systemic oxidative stress can be ascribed to the reductive property of H_2 gas. The formation of 4-hydroxynonenal (HNE) through lipoprotein oxidation plays an etiologic role in atherosclerotic lesion progression [14,15]. Oxidized LDL is taken up by macrophages through scavenger receptors, to form foam cells. Foam cells secrete growth factors that induce SMC migration from the media into the neointima. We demonstrate that the ingestion of H_2-dissolved water *ad libitum* for 6 months prevents the development of atherosclerosis in apolipoprotein E-knockout mice, which represent a model of spontaneously developing atherosclerosis [16]. This anti-atherogenic effect of H_2-dissolved water is associated with a reduction of HNE immunoreactivity in the aorta. These results suggest that persistent intake of H_2 has the potential to reduce oxidative stress and may prevent cardiovascular disease.

3. Unexpected benefit of flatulence caused by α-glucosidase inhibitors

Is there any other way to supply H_2 to the body? H_2 is not produced endogenously in mammalian cells, since the hydrogenase activity responsible for the formation of H_2 gas may not be present [17]. Instead, spontaneous production of H_2 gas in the human body occurs *via* the fermentation of undigested carbohydrates by the resident enterobacterial flora. H_2 is transferred to the portal circulation and excreted through the breath in significant amounts [18]. Flatulence is regarded as the major side-effect of treatment with α-glucosidase inhibitors [19]. Therefore, we examined whether the administration of α-glucosidase inhibitors increases the levels of H_2 production in the gastrointestinal tract. Eleven healthy volunteers (10 males and 1 female) were administered acarbose at a dosage of 300 mg/day (100 mg three times a day) for 4 days under free-feeding conditions (Table 1). On Day 4 of the experiment, the levels of exhaled H_2 and methane (CH_4) were measured using the Breath Gas Analyzer Model TGA-2000 (TERAMECS, Kyoto, Japan). Acarbose treatment significantly increased the amount of exhaled H_2 at every time-point examined ($n = 11$, $P < 0.05$, paired t-test, as compared to before treatment with acarbose), whereas it had modest effects on CH_4 production (Fig. 1). Acarbose treatment had no effect on H_2 or CH_4 production in 2/11 volunteers.

Kajiyama treated patients with type 2 diabetes or impaired glucose tolerance with 900 ml/day (300 ml three times a day) H_2-dissolved water. After drinking 300 ml of H_2-dissolved water, the exhaled H_2 gas concentration reached a maximum of 56 ± 27.8 ppm at 15 min, and returned to the baseline level at 150 min. This peak level of H_2 gas reduced the levels of oxidative stress biomarkers and improved glucose metabolism in patients with type 2 diabetes or impaired glucose tolerance [13]. In the present study, we show that oral administration of acarbose at a dosage of 300 mg/day (100 mg given three times a day) can reach

Table 1
Eleven healthy volunteers (10 males and 1 female) were administered acarbose at a dosage of 300 mg/day (100 mg three times a day) for 4 days under free-feeding conditions. Exhaled gas was collected in an aluminium bag at the point of mid-expiration at the indicated time-points (i.e., morning, before lunch, 2 h after lunch, before retiring), both before and after acarbose treatment. The exhaled gas samples were injected into the Breath Gas Analyzer to measure the H_2 and CH_4 concentrations.

Sex	Hydrogen								Methane							
	Before				After				Before				After			
	Morning	Before lunch	After lunch	Before retiring	Morning	Before lunch	After lunch	Before retiring	Morning	Before lunch	After lunch	Before retiring	Morning	before lunch	After lunch	Before retiring
M	1	2	11	10	34	21	74	90	0	3	2	2	8	3	9	9
M	8	6	3	1	17	25	48	19	4	4	2	2	4	4	6	3
M	46	14	20	20	76	32	52	56	5	2	2	3	7	4	5	6
M	3	6	3	8	85	44	58	91	23	34	20	19	11	9	8	12
M	43	31	25	10	64	62	62	45	4	32	2	2	8	6	6	5
M	8	3	9	13	20	24	40	41	1	1	3	5	4	4	5	7
M	37	15	17	11	30	53	46	38	5	2	1	1	5	5	3	5
F	10	30	32	29	54	15	14	30	2	8	7	8	11	7	6	7
M	15	2	5	6	26	20	33	11	5	1	1	2	7	6	8	4
M	52	44	56	42	38	54	31	49	18	15	18	17	10	16	12	16
M	5	5	1	21	3	5	21	70	11	22	14	44	29	27	38	50

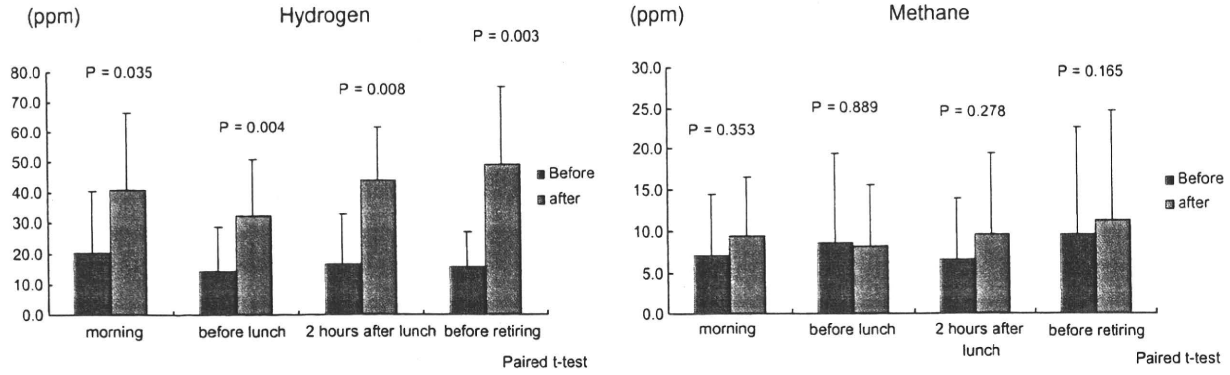

Fig. 1. Effects of acarbose on the levels of exhaled H_2 and CH_4. The values shown in the bar graphs are means ± S.D.

the same maximum levels of exhaled H_2 gas as compared to the consumption of 300 ml of H_2-dissolved water. Moreover, acarobose maintained this peak level continuously. It is noteworthy that the breath concentration of H_2 on a fasting morning remains high in people who take acarbose. These observations clearly indicate that the amounts of H_2 gas generated by acarbose in our current experiments are sufficient to reduce systemic oxidative stress. Oral administration of acarbose may be superior to drinking H_2-rich water in terms of maintenance of the appropriate H_2 gas levels in the body.

4. Conclusion

Based on these observations and experimental results, we propose that α-glucosidase inhibitors reduce the risk of cardiovascular disease in patients with impaired glucose tolerance or type 2 diabetes, and that these benefits can be attributed at least in part to the abilities of these drugs to neutralise oxidative stress by increasing the production of H_2 in the gastrointestinal tract. To investigate the relationship between the cardiovascular benefits of α-glucosidase inhibitors and H gas production by the gut microbiota, we should examine whether the cardiovascular benefits afforded by these drugs are diminished by scavenging H_2 gas in the gastrointestinal tract before absorption into the blood stream.

Conflict of interest statement

None declared.

Acknowledgement

This work was supported by a PRESTO (Metabolism and Cellular Function) Grant from the Japan Science and Technology Agency to M. Sano.

References

[1] Coutinho, M., Gerstein, H.C., Wang, Y. and Yusuf, S. (1999) The relationship between glucose and incident cardiovascular events. A metaregression analysis of published data from 20 studies of 95,783 individuals followed for 12.4 years. Diabetes Care 22, 233–240.
[2] Barrett-Connor, E. and Ferrara, A. (1998) Isolated postchallenge hyperglycemia and the risk of fatal cardiovascular disease in older women and men. The rancho bernardo study. Diabetes Care 21, 1236–1239.
[3] Chiasson, J.L., Josse, R.G., Gomis, R., Hanefeld, M., Karasik, A. and Laakso, M. (2003) Acarbose treatment and the risk of cardiovascular disease and hypertension in patients with impaired glucose tolerance: the STOP-NIDDM trial. JAMA 290, 486–494.
[4] Hanefeld, M., Cagatay, M., Petrowitsch, T., Neuser, D., Petzinna, D. and Rupp, M. (2004) Acarbose reduces the risk for myocardial infarction in type 2 diabetic patients: meta-analysis of seven long-term studies. Eur. Heart J. 25, 10–16.
[5] (1998) Intensive blood-glucose control with sulphonylureas or insulin compared with conventional treatment and risk of complications in patients with type 2 diabetes (UKPDS 33). UK Prospective Diabetes Study (UKPDS) Group. Lancet 352, 837–853.
[6] Frantz, S., Calvillo, L., Tillmanns, J., Elbing, I., Dienesch, C., Bischoff, H., Ertl, G. and Bauersachs, J. (2005) Repetitive postprandial hyperglycemia increases cardiac ischemia/reperfusion injury: prevention by the α-glucosidase inhibitor acarbose. FASEB J. 19, 591–593.
[7] Madamanchi, N.R., Hakim, Z.S. and Runge, M.S. (2005) Oxidative stress in atherogenesis and arterial thrombosis: the disconnect between cellular studies and clinical outcomes. J. Thromb. Haemost. 3, 254–267.
[8] Touyz, R.M. (2004) Reactive oxygen species, vascular oxidative stress, and redox signaling in hypertension: what is the clinical significance? Hypertension 44, 248–252.
[9] Wilcox, C.S. (2003) Redox regulation of the afferent arteriole and tubuloglomerular feedback. Acta Physiol. Scand. 179, 217–223.
[10] Steinhubl, S.R. (2008) Why have antioxidants failed in clinical trials? Am. J. Cardiol. 101, 14D–19D.
[11] Ohsawa, I. et al. (2007) Hydrogen acts as a therapeutic antioxidant by selectively reducing cytotoxic oxygen radicals. Nat. Med. 13, 688–694.
[12] Hayashida, K. et al. (2008) Inhalation of hydrogen gas reduces infarct size in the rat model of myocardial ischemia-reperfusion injury. Biochem. Biophys. Res. Commun. 373, 30–35.
[13] Kajiyama, S. et al. (2008) Supplementation of hydrogen-rich water improves lipid and glucose metabolism in patients with type 2 diabetes or impaired glucose tolerance. Nutr. Res. 28, 137–143.
[14] Lusis, A.J. (2000) Atherosclerosis. Nature 407, 233–241.
[15] Berliner, J.A. and Watson, A.D. (2005) A role for oxidized phospholipids in atherosclerosis. N Engl. J. Med. 353, 9–11.
[16] Ohsawa, I., Nishimaki, K., Yamagata, K., Ishikawa, M. and Ohta, S. (2008) Consumption of hydrogen water prevents atherosclerosis in apolipoprotein E knockout mice. Biochem. Biophys. Res. Commun. 377, 1195–1198.
[17] Adams, M.W., Mortenson, L.E. and Chen, J.S. (1980) Hydrogenase. Biochim. Biophys. Acta 594, 105–176.
[18] Levitt, M.D. (1969) Production and excretion of hydrogen gas in man. N Engl. J. Med. 281, 122–127.
[19] Ladas, S.D., Frydas, A., Papadopoulos, A. and Raptis, S.A. (1992) Effects of α-glucosidase inhibitors on mouth to caecum transit time in humans. Gut 33, 1246–1248.

Biochemical and Biophysical Research Communications 387 (2009) 353–359

Contents lists available at ScienceDirect

Biochemical and Biophysical Research Communications

journal homepage: www.elsevier.com/locate/ybbrc

Omentopexy enhances graft function in myocardial cell sheet transplantation

Ryo Suzuki [a,b], Fumiyuki Hattori [a], Yuji Itabashi [a], Masatoyo Yoshioka [a], Shinsuke Yuasa [a], Haruko Manabe-Kawaguchi [a], Mitsushige Murata [a], Shinji Makino [a], Kiyokazu Kokaji [b], Ryohei Yozu [b], Keiichi Fukuda [a,*]

[a] Department of Regenerative Medicine and Advanced Cardiac Therapeutics, Keio University School of Medicine, Tokyo, Japan
[b] Department of Cardiovascular Surgery, Keio University School of Medicine, Tokyo, Japan

ARTICLE INFO

Article history:
Received 3 June 2009
Available online 10 July 2009

Keywords:
Myocardial cell sheet
Transplant
Infarct
Regenerative medicine
Omentopexy

ABSTRACT

Myocardial cell sheets (MCS) are a potentially valuable tool for tissue engineering aimed at heart regeneration. Several methods have recently been established for the fabrication of MCS. However, the lack of a sufficient blood supply has inhibited functional recovery of the MCS. To address this challenge, we combined MCS transplantation with omentopexy (OP), which utilizes omental tissue as a surgical flap. Rats were divided into five groups: sham, myocardial infarction (MI), MCS transplantation, OP, and MCS + OP. Histologic analysis revealed that MCS + OP drastically reversed MI-induced cardiac remodeling. Echocardiography revealed that MCS increased cardiac function, while OP had a synergistic beneficial effect with MCS transplantation. Immunofluorescence imaging showed that OP increased the survival of transplanted cardiomyocytes, and increased the blood supply through enhancement of angiogenesis and migration of small arteries into the MCS. Taken together, we concluded that OP is a promising strategy for the enhancement of graft function in MCS transplantation.

Recent studies in regenerative medicine have achieved major successes in generating human cardiomyocytes from tissue-specific stem cells, embryonic stem (ES) cells, and induced pluripotent stem (iPS) cells [1,2]. However, it remains unclear as to how these regenerative cells can be transplanted into the heart *in vivo*. A clinical trial involving myocardial injection of autologous myoblasts produced a limited but important recovery of cardiac function [3]. However, the direct delivery of isolated cells or delivery *via* the coronary vessels can induce both aggregation and coagulative necrosis of the grafted cells. We and others have reported that needle injection of regenerative cardiomyocytes into beating intramyocardial tissues results in poor cell survival rates, with fewer than 5% of the regenerated cardiomyocytes surviving transplantation [1,4]. The establishment of cell transplantation techniques that ensure cell survival is therefore a priority.

Shimizu and colleagues have developed a new technique for the fabrication of myocardial cell sheets (MCS) using temperature-responsive culture dishes [5]. This technique enables the generation of three-dimensional, thin myocardial tissues. We have also developed a novel technique for the easy production of MCS using fibrin polymer-coated dishes [6]. These techniques facilitate cell sheet fabrication. In addition, we have demonstrated that transplantation of three-layered MCS into the dorsal subcutaneous tissues of rats lead to the formation of spontaneously beating heart tissues with appropriate structure and sarcomere striation [6]. In this study, newly developed small vessels entered the transplanted MCS from the surrounding soft connective tissue.

We also transplanted three-layered MCS onto an infarcted heart *in vivo*, and found that the transplanted tissues were beating in synchrony with the surrounding heart tissue 1 week after transplantation [7]. However, the transplantation of MCS onto the surface of the ventricular wall was distinct from that into the subcutaneous tissue. The development of newly formed vessels from the coronary arteries or myocardial tissue *in situ* was limited, and the blood supply for the MCS was insufficient, which hindered the long-term maintenance of the thick MCS.

The omentum (OM) is an attractive tissue for use in cardiac surgery, as it is highly vascularized, providing oxygen and nutrients, and it acts as a source of angiogenesis factors [8]. Prior to the development of coronary artery bypass graft procedures, cardio-omentopexy (OP) was applied to ischemic areas of the human heart [9]. Vineberg and colleagues have introduced a modified OP, in which the OM is used as a pedicle flap to attach to the left ventricle, which is then connected with an internal mammary artery [10]. Although these classic techniques for treating angina pectoris require long periods of time for the maturation of graft-coronary communication, favorable results have been reported in several studies [11].

* Corresponding author. Address: Department of Regenerative Medicine and Advanced Cardiac Therapeutics, Keio University School of Medicine, 35 Shinanomachi, Shinjuku-ku, Tokyo 160-8582, Japan. Fax: +81 3 5363 3875.
E-mail address: kfukuda@sc.itc.keio.ac.jp (K. Fukuda).

0006-291X/$ - see front matter © 2009 Elsevier Inc. All rights reserved.
doi:10.1016/j.bbrc.2009.07.024

We investigated the use of OM as the source of a blood supply for MCS transplantation. We also investigated whether the combination of OP and MCS transplantation is effective in preserving the transplanted cardiomyocytes and augmenting heart functions.

Methods

Experimental animals. Eight-week-old, T-cell-deficient F344/NJcl-rnu/rnu (Nude) rats were purchased from Japan CLEA (Tokyo, Japan). Neonatal GFP-transgenic rats were purchased from Japan SLC (Shizuoka, Japan). All experimental procedures and protocols were approved by the Animal Care and Use Committee of Keio University, Japan.

Manipulation of the MCS. Polymerized fibrin-coated dishes were prepared as described previously [6]. Briefly, Tissiel™ (Baxter, Vienna, Austria) was mixed with 90 mg human fibrinogen, 20 mg human serum, 0.4 U thrombin, 0.59 mg $CaCl_2$ ($2H_2O$), and 3000 U aprotinin. The solution was diluted with 16 mL of saline, and 0.3-mL aliquots were rapidly spread onto 35-mm culture dishes. Two hours later, the polymerized fibrin-coated dishes were ready for use.

Primary cultures of cardiomyocytes were prepared from the ventricles of 1-day-old GFP-transgenic rats, as described previously [12], and plated onto the fibrin-coated dishes ($5.6 \times 10^5/cm^2$). The MCS were easily dissociated in intact form from the polymerized fibrin layer [6]. After 4 days, the MCS were detached from the surfaces of the dishes using a cell scraper, laid flat on culture medium (199/DMEM supplemented with 10% FBS), trimmed to a square shape, gently aspirated into the tip of a 10-ml pipette, and then transferred onto a culture surface with the same square shape as the MCS. Once in place, medium was dropped onto the center of the sheet, to spread the folded parts of the transferred MCS. After sheet spreading, the medium was aspirated, so as to promote adherence of the cell sheets to one another. Thus, it was possible to overlay the sheets in a triple layer. As the cell sheets were relatively fragile, they were mounted onto a collagen film (CM-6; Koken, Tokyo, Japan) before transplantation [7]. The MCS mounted on the collagen film were easily delivered to the heart, and once the sheets were placed in the area of induced ischemia, the collagen film was removed and the MCS were retained on the heart surface (Fig. 1A and C). After a few minutes, the MCS adhered tightly to the heart surface.

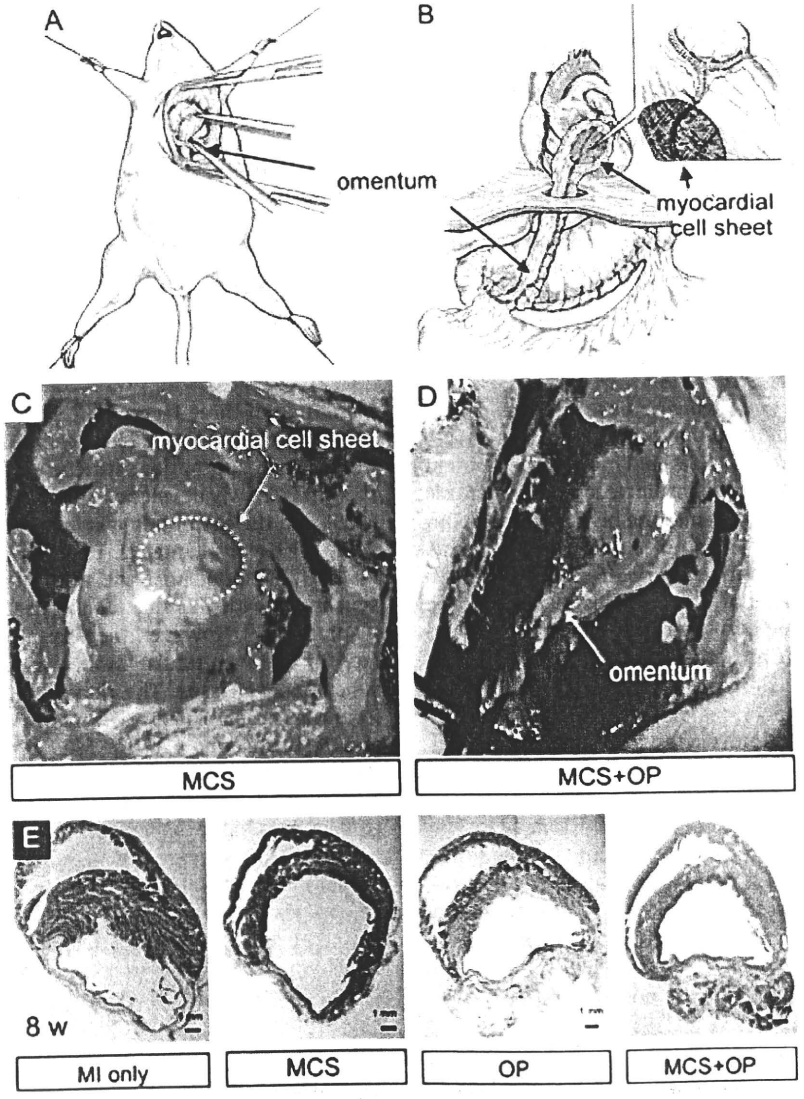

Fig. 1. Representative schemas and operator's views of myocardial cell sheet (MCS) transplantation and omentopexy (OP). (A, B) MCS transplantation and OP operation schemas. (C) Seven days after MCS transplantation. The MCS is attached to the surface of the infarcted area. (D) Seven days after MCS + OP. The omental flap is tightly bound to the MCS-transplanted area. (E) Representative short-axis sections of hearts 8 weeks post-surgery in (1) the myocardial infarction (MI) only group, (2) the MCS groups, (3) the OP group, and (4) the MCS + OP groups.

Generating myocardial infarction rat models. Male, 8-week-old, nude rats were anesthetized by inhalation of 1% sevoflurane (Maruishi Pharmaceutical, Osaka, Japan) and maintained on a ventilator (Natsume, Tokyo, Japan). After the induction of anesthesia, the rats were given a subcutaneous injection of 1% procaine–HCl (5–10 ml) (AstraZeneca, London, UK). The initial step of the surgical procedure was the opening and exposure of the heart by a left 3rd intercostal space incision. MI was induced by ligation of the left descending coronary artery with 6-0 Prolene (Ethicon) at the left appendage area.

Omental tissue preparation. We performed an upper midline laparotomy, and then manipulated the omental tissue in a way of pedicle flap, and that flap was reached to pleural cavity through transdiaphragmatic approach (making a small hole in the diaphragm), and wrapped directly around the anterior wall in which the MI had been produced and the MCS had been transplanted in advance (Fig. 1B and D).

Experimental design. Rats were randomized to five groups: sham operation ($n = 5$, data not shown), isolated MI group ($n = 10$), MCS group ($n = 10$), OP group ($n = 10$), and MCS + OP group ($n = 10$). For the post-operative evaluations, we performed echocardiography at 1, 4, and 8 weeks. Rats were anesthetized with pentobarbital, and sacrificed after 1 week or 8 weeks.

Echocardiography and hemodynamic measurements. Rats were anesthetized with ketamine (30 mg/kg) and xylazine (6 mg/kg), so as to maintain spontaneous breathing. Echocardiography (ECG) was performed as described previously [13], using the Image Point 1500 (Philips) with a 15-MHz transducer.

Histologic analysis and immunofluorescence imaging. After anesthesia, the rat hearts were perfused from the apex with PBS, perfusion-fixed with 4% paraformaldehyde (PFA)/PBS, and used for immunostaining, as described previously [1]. The sections were incubated overnight at 4 °C with affinity-purified rabbit polyclonal anti-GFP (1:100 dilution, MBL598; Medical & Biological Laboratories, Japan), rabbit polyclonal anti-VEGF-A (1:200 dilution, sc-507; Santa Cruz Biotechnology), anti-von Willebrand factor (1:200 dilution, vWF, RB-281-A0; Lab Vision), and mouse monoclonal anti-sarcomeric actinin (1:400 dilution; Sigma–Aldrich). Then, the sections were incubated with secondary antibodies conjugated with Alexa 594 (Invitrogen). Nuclei were stained with TOTO-3 (Invitrogen). The slides were observed under a confocal laser-scanning microscope (LSM 510 META; Carl Zeiss, Jena, Germany). Optical sections were obtained at resolutions of 512 × 512 to 1024 × 1024 pixels, and analyzed using the LSM software (Carl Zeiss).

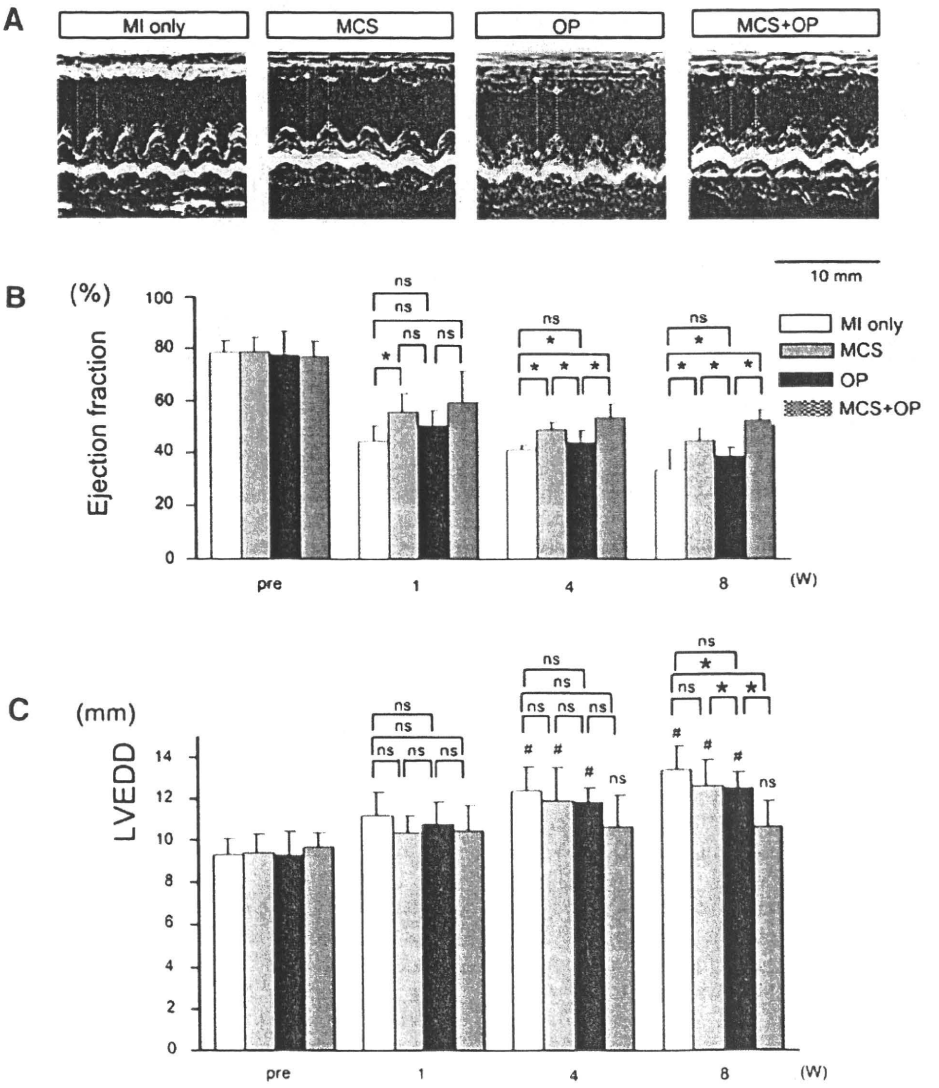

Fig. 2. Effects of MCS and MCS + OP on the functions of infarcted hearts, as examined by echocardiography. (A) M-mode echocardiography of the left ventricle (at the papillary muscle level). (B) Time course of the ejection fraction of (1) the myocardial infarction (MI) only group, (2) the MCS groups, (3) the OP group, and (4) the MCS + OP groups. (C) Time course of the left ventricular end-diastolic diameters of each group. Data shown are means ± SD. $P < 0.05$ for comparison of two groups; $^{\#}P < 0.05$ vs. pre-operative samples; ns, not significant.

Statistical analysis. Values are presented as means ± SD. Statistical significance was evaluated using the unpaired Student's *t*-test for comparisons between two mean values. Multiple comparisons between more than three groups were performed using the non-parametric Dunnett's multiple comparison tests. A *P*-value of <0.05 was considered statistically significant.

Results

MCS transplantation with or without omentopexy

To investigate whether MCS transplantation or MCS transplantation combined with OP is effective at improving cardiac function, we first transplanted three overlaid MCS onto the ischemic area of the left ventricle, in some group, OP was also transplanted onto the MCS. When we opened the chest 1 week after the operation we found that the MCS graft was beating synchronously with the host heart. However, the OM tissue largely adhered to the thoracic wall in the MCS + OP group. We carefully detached the OM tissue from the thoracic wall, and observed that the MCS was entirely covered by the OP (Fig. 1D). Fig. 1E shows a representative cross-section of the left ventricle at the papillary muscle level 8 weeks after the operation. The infarcted area in the MI group showed marked thinning and elongation, while that in the MCS group showed the less degree of thinning and elongation. Interestingly, the OP group also inhibited remodeling effect, similarly to the MCS group. Moreover, the infarcted area of the MCS + OP group showed synergistic improvements in thinning and elongation. These findings suggest that the MCS alone improves the function of the infarcted heart, and that OP enhances the reverse remodeling effect of the MCS.

Echocardiographic findings

We performed two-dimensional and M-mode echocardiography for the evaluation (Fig. 2A). In the MI group, the short-axis view revealed akinesis of the anterior wall and dilatation of the LV. In contrast, the MCS group showed hypokinesis of the anterior wall and slightly decreased LV dilatation. The MCS + OP group showed further improvement of wall motion and prevention of dilatation.

The ejection fraction (EF) and LV end-diastolic diameter were quantitated (Fig. 2B and C). In the MI group, the EF decreased to 40% and the LV was dilatated at 1 week, and these features deteriorated in a time-dependent manner, suggesting remodeling of the infarcted heart. In the MCS group, the EF was significantly improved by 15% and LV dilatation was slightly improved at 1 week. These reverse remodeling effects were more prominent at the late stage. In the OP group, the EF was not rescued but LV dilatation was slightly rescued at the late stage, indicating that the OP mechanically supported the infarcted wall and enhanced reverse remodeling at the late stage. In the MCS + OP group, the EF was markedly improved and LV dilatation was markedly prevented. Thus, the combination of MCS transplantation and OP acts synergistically, rather than additively, on cardiac reverse remodeling.

Although MCS was effective at improving cardiac function, it was not sufficient to prevent the deterioration of cardiac function in the long-term. Moreover, although OP alone was not sufficient in this respect, the combination of MCS transplantation and OP not only improved cardiac function, but also induced reverse remodeling of the infarcted heart.

Histologic analyses of MCS and MCS+OP transplantation

To examine further why the combination of MCS and OP had a synergistic effect on the reversal of cardiac remodeling, we performed histologic analyses. Initially, we investigated the quality of the grafted cardiomyocytes. For that, we evaluated the sarcomeric actinin-positive cardiomyocytes fraction in GFP-positive cells populations between the MCS and MCS + OP groups by immunofluorescence imaging. We found that a significantly higher number of cardiomyocytes survived in the MCS + OP group than in the MCS group, and that the individual cardiomyocytes were larger in the MCS + OP group than in the MCS group (Fig. 3). Thus, OP had beneficial effects in terms of the survival and maintenance of the transplanted MCS.

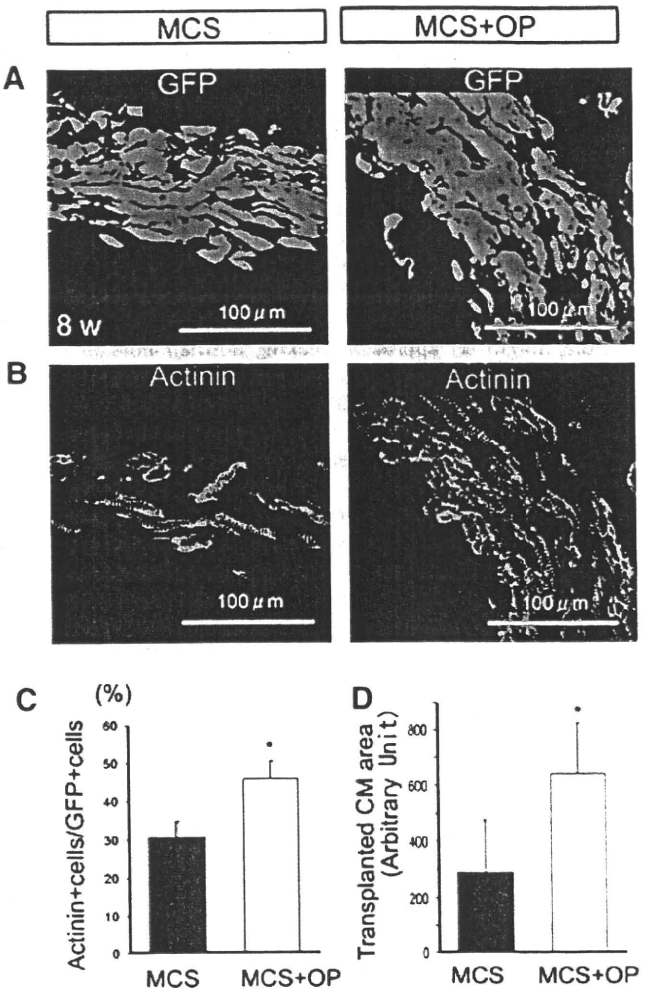

Fig. 3. (A, B) Immunofluorescence imaging of the MCS-transplanted heart for GFP (green) and α-actin (red). Note that the transplanted MCS is thicker in the MCS + OP group than in the MCS group. (C) Quantitative analysis of actinin-positive cells in the GFP-positive cell populations. The number of surviving cardiomyocytes is higher in the MCS + OP group than in the MCS group. (D) Quantitative analysis of the cardiomyocyte-positive areas in the two groups. Data shown are means ± SD. $^{*}P < 0.05$, for comparison of the two groups.

To investigate the mechanisms underlying the beneficial effects of OP on MCS, we examined how OP contributed to cardiac function. We compared the numbers of vessels in the MCS and MCS + OP groups at 1 week post-operatively (Fig. 4A). Initially, we observed the MCS and infarcted area using HE staining. In accordance with the results shown in Fig. 3, the thickness of the MCS was increased in the MCS + OP group, as compared with that in the MCS group (Fig. 4A and B). Interestingly, we found that many more small vessels had migrated into the MCS in the MCS + OP group than in the MCS group. Quantitative analysis of the small vessels (Fig. 4C) showed that the number of small vessels in the MCS + OP group was about 3.4-fold higher than that in the MCS

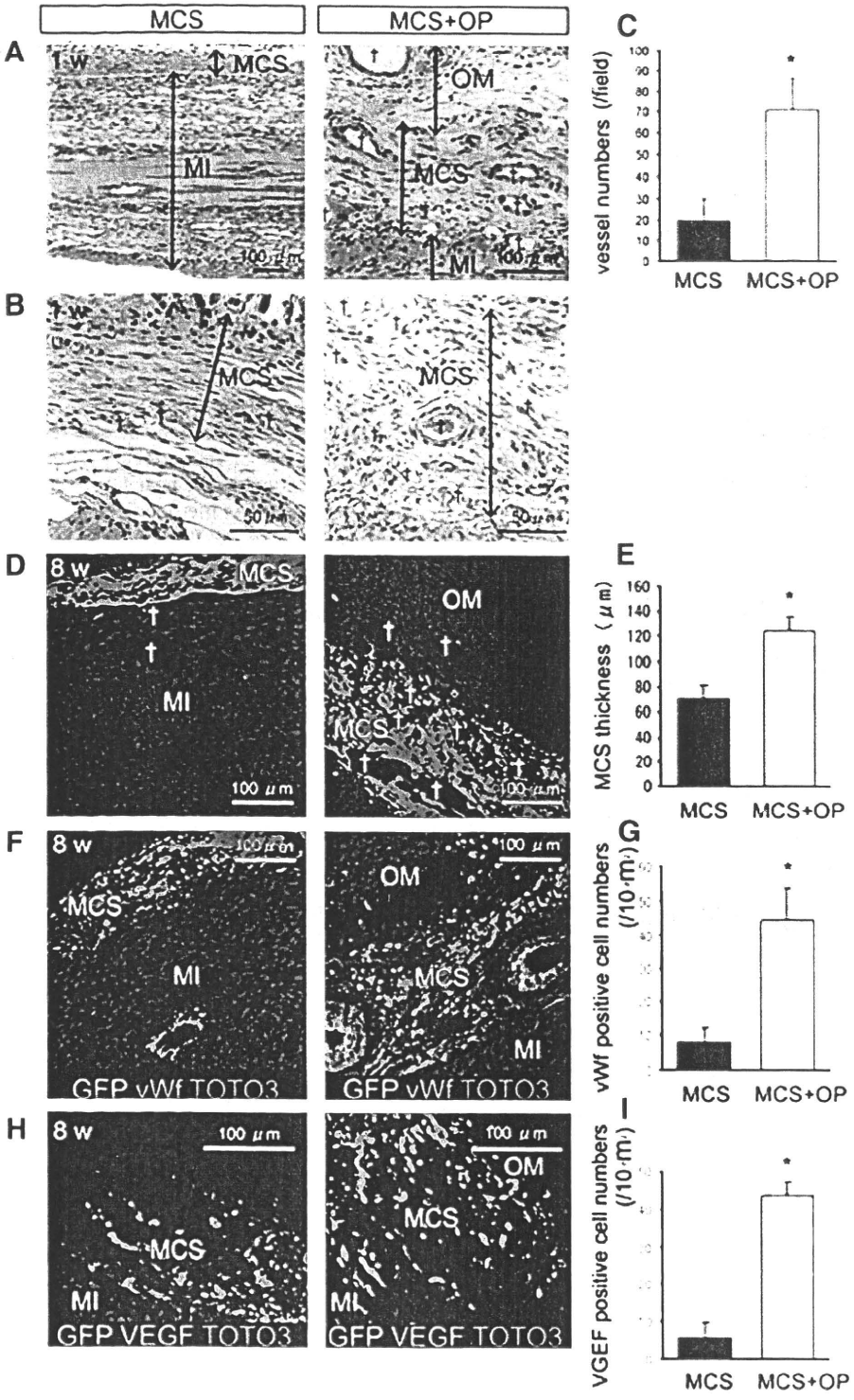

Fig. 4. Histologic and immunohistologic analyses of the MCS and MCS + OP transplants into infarcted hearts. In all cases, the left and right figures represent MCS and MCS + OP, respectively. (A, B) Representative histologies of the MCS and MCS + OP groups at 1 week post-transplantation; HE staining. MI, myocardial infarcted area; MCS, myocardial cell sheet; OM, omental tissue. Note that the MCS is thicker in the MCS + OP group than in the MCS group, and that there are more small vessels (†) in the MCS + OP group. (C) Quantitative analysis of vessel numbers. (D) Investigation of MCS thickness by immunofluorescence imaging. Immunohistologic detection of vWF (F) and VEGF (H) within the transplanted MCS, comparing the MCS and MCS + OP groups. (C, E, G, and I) These results were shown in bar graphs. $^{*}P < 0.05$.

group. In the MCS group, several capillary-level vessels were located either at the border between the MCS and the infarcted area or within the MCS. In contrast, in the MCS + OP group, large numbers of capillary-level and small arteriole-level vessels were located in proximity to the border between the MCS and OM or within the MCS (Fig. 4B), which suggests that the MCS receives its blood supply directly from not only the infarcted area, but also the omentum, which seems to be a more robust source of blood.

To examine the long-term effect of OP on MCS transplantation, we performed immunofluorescence imaging at 8 weeks. The thickness of the MCS was greater in the MCS + OP group than in the MCS group (Fig. 4D). Quantitative analysis showed that the thickness of

the MCS was about 1.7-fold greater in the MCS + OP group than in the MCS group (Fig. 4E). We found that the omental tissue infiltrated the MCS, and numerous vessel lumens were detected in the MCS + OP group.

Immunofluorescence staining for vWF and VEGF revealed that only the MCS group contained capillary-level vessels, while the MCS + OP group contained arteriole-level vessels within the MCS. The number of vWF-positive cells within the MCS was 9-fold higher in the MCS + OP group than in the MCS group (Fig. 4G).

The immunofluorescence staining showed that many VEGF-positive cells had infiltrated the MCS with OP. Interestingly, most of the VEGF-positive cells were GFP-negative, indicating that they originated from the omentum. Quantitative analysis revealed that the number of VEGF-positive cells was 9-fold higher in the MCS + OP group than in the MCS group (Fig. 4I).

Taken together, our results indicate that OP stimulates not only the migration of VEGF-positive cells, but also the development or invasion of arteriole-level small vessels into the MCS, thereby contributing to the survival and maintenance of transplanted MCS.

Discussion

In the present study, we investigated the potential benefits of MCS transplantation into the infarcted heart, as well as the effect of OP on the maintenance of transplanted MCS. MCS transplantation prevented cardiac remodeling and improved cardiac function, as compared with the isolated MI group. However, we also found that MCS transplantation alone did not maintain the MCS in good condition, owing to an insufficient blood supply. Only a few small vessels migrated into the MCS from the epicardial side, which limited cardiomyocyte survival.

In contrast, OP strongly reversed cardiac remodeling and synergistically improved the functionality of the infarcted myocardium. We investigated the mechanisms by which the combination of OP and MCS synergistically improved cardiac function, and found that OP promoted the migration of not only capillaries, but also sufficient numbers of arteriole-level small vessels, thereby increasing the number of cardiomyocytes surviving in the MCS and inducing physiologic hypertrophy of the transplanted cardiomyocytes. Indeed, the thickness of the cell sheet for MCS combined with OP was greater than that seen for MCS transplantation alone.

Previously, OP was reported as a source of capillary vessels and large arterioles and was implicated in the maturation of new blood vessels, in similarity to arteriogenesis, which is defined as the rapid proliferation of pre-existing collateral arteries [14]. As demonstrated in our current immunofluorescence imaging, the OM contains and secretes the largest amount of VEGF, as compared with other adipose tissues, and hypoxia induces VEGF expression in omental adipocytes at the transcriptional level [8]. Recently, Ueyama and colleagues [15] demonstrated that bypass from the gastroepiploic artery in the OM to the native coronary artery could be achieved by the administration of slow-release basic fibroblast growth factor without surgical anastomosis. Moreover, a recent study has shown vascular communication between vessels in the omental flap and native coronary artery using angiography while flushing the contrast dye from the left gastroepiploic artery [14]. Thus, the OM was used previously as a flap to provide a blood supply to the heart in patients with multiple diffuse coronary artery sclerosis. Unfortunately, this proved unsuccessful, probably due to the existence of epicardium and incomplete revascularization. Sekiya and coworkers recently demonstrated that graft-derived endothelial cells created fused vessels with host endothelial cells at the border between the host and graft cells [16]. However, these vascular communications were established between the grafted MCS and dorsal subcutaneous tissues rather than the surface of the ventricular wall. We assumed that the epicardium would prevent the migration of arteriole-level blood vessels. However, we found that OP supplied a sufficient number of blood vessels directly to the MCS. Presumably, the MCS did not contain the epicardium, which made it easy to distribute numerous vessels into the MCS. Since the border between the MCS and omental tissue was not clearly observed by HE staining, eventually we need to use neonatal GFP rat cardiomyocytes as the donor cells.

Overall, OP appears to be an ideal source of a blood supply for the transplanted MCS. Furthermore, we strongly believe that these omental effects are significant contributing factors to reverse remodeling of the MI region. In addition, previous lines of evidence indicate that OP limits infarct size, which contributes to differences in ventricle size that are related to alteration of the remodeling process [15].

Given the ongoing development of regenerative medicine, MCS-based heart regeneration therapy is sure to play a pivotal role in the treatment of severe heart failure, as an alternative to heart transplantation, in the near future. For this to succeed, it is necessary to pursue the methodologic progress that facilitate cell transplantation with a sufficient blood supply.

Currently, we are able to regenerate human cardiomyocytes from ES and iPS cells [17]. The next step is the development of methodologic options for delivering these cardiomyocytes in the form of a natural living tissue.

Disclosures

None.

Acknowledgments

This study was supported in part by research grants from the Ministry of Education, Culture, Sports, Science and Technology, Japan, and the Program for Promotion of Fundamental Studies in Health Sciences of the National Institute of Biomedical Innovation (NIBIO).

References

[1] N. Hattan, H. Kawaguchi, K. Ando, E. Kuwabara, J. Fujita, M. Murata, M. Suematsu, H. Mori, K. Fukuda, Purified cardiomyocytes from bone marrow mesenchymal stem cells produce stable intracardiac grafts in mice, Cardiovasc. Res. 65 (2005) 334–344.
[2] S. Makino, K. Fukuda, S. Miyoshi, F. Konishi, H. Kodama, J. Pan, M. Sano, T. Takahashi, S. Hori, H. Abe, J. Hata, A. Umezawa, S. Ogawa, Cardiomyocyte can be generated from marrow stromal cells in vitro, J. Clin. Invest. 103 (1999) 697–705.
[3] P. Menasche, A.A. Hagege, M. Scorsin, B. Pouzet, M. Desnos, D. Duboc, K. Schwartz, J.T. Vilquin, J.P. Marolleau, Myoblast transplantation for heart failure, Lancet 357 (2001) 279–280.
[4] M. Zhang, D. Methot, V. Poppa, Y. Fujio, K. Walsh, C.E. Murry, Cardiomyocyte grafting for cardiac repair: graft cell death and anti-death strategies, J. Mol. Cell Cardiol. 33 (2001) 907–921.
[5] T. Shimizu, M. Yamato, Y. Isoi, T. Akutsu, T. Setomaru, K. Abe, A. Kikuchi, M. Umezu, T. Okano, Fabrication of pulsatile cardiac tissue grafts using a novel 3-dimensional cell sheet manipulation technique and temperature-responsive cell culture surface, Circ. Res. 90 (2002) e40.
[6] Y. Itabashi, S. Miyoshi, H. Kawaguchi, S. Yuasa, K. Tanimoto, A. Furuta, T. Shimizu, T. Okano, K. Fukuda, S. Ogawa, A new method for manufacturing cardiac cell sheets using fibrin-coated dishes and its electrophysiological studies by optical mapping, Artif. Organs 29 (2005) 95–103.
[7] A. Furuta, S. Miyoshi, Y. Itabashi, T. Shimizu, S. Kira, K. Hayakawa, N. Nishiyama, K. Tanimoto, Y. Hagiwara, T. Satoh, K. Fukuda, T. Okano, S. Ogawa, Pulsatile cardiac tissue grafts using a novel three-dimensional cell sheet manipulation technique functionally integrates with the host heart, in vivo, Circ. Res. 98 (2006) 705–712.
[8] Q.X. Zhang, C.J. Magovern, C.A. Mack, K.T. Budenbender, W. Ko, T.K. Rosengart, Vascular endothelial growth factor is the major angiogenic factor in omentum: mechanism of the omentum-mediated angiogenesis, J. Surg. Res. 67 (1997) 147–154.
[9] L. O'Shaughnessy, Surgical treatment of cardiac ischemia, Lancet 232 (1937) 185–194.
[10] A.M. Vineberg, Y. Kato, W.J. Pirozynski, Experimental revascularization of the entire heart. Evaluation of epicardiectomy, omental graft, and/or implantation

of the internal mammary artery in preventing myocardial necrosis and death of the animal, Am. Heart J. 72 (1966) 79–93.
[11] J.W. Streider, H.M. Clute, A. Graubiel, A Cardioomentopexy in the treatment of angina pectoris, N. Eng. J. Med. 222 (1940) 41–43.
[12] H. Kodama, K. Fukuda, J. Pan, S. Makino, A. Baba, S. Hori, S. Ogawa, Leukemia inhibitory factor, a potent cardiac hypertrophic cytokine, activates the JAK/STAT pathway in rat cardiomyocytes, Circ. Res. 81 (1997) 656–663.
[13] D.J. Sahn, A. DeMaria, J. Kisslo, A. Weyman, Recommendations regarding quantitation in M-mode echocardiography: results of a survey of echocardiographic measurements, Circulation 58 (1978) 1072–1083.
[14] T. Kanamori, G. Watanabe, T. Yasuda, H. Nagamine, H. Kamiya, Y. Koshida, Hybrid surgical angiogenesis: omentopexy can enhance myocardial angiogenesis induced by cell therapy, Ann. Thorac. Surg. 81 (2006) 160–168.
[15] K. Ueyama, G. Bing, Y. Tabata, M. Ozeki, K. Doi, K. Nishimura, H. Suma, M. Komeda, Development of biologic coronary artery bypass grafting in a rabbit model: revival of classic concept with modern biotechnology, J. Thoracic Cardiovasc. Surg. 127 (2004) 1608–1615.
[16] S. Sekiya, T. Shimiz, M. Yamato, A. Kikuchi, T. Okano, Bioengineered cardiac cell sheet grafts have intrinsic angiogenic potential, Biochem. Biophys. Res. Commun. 341 (2006) 573–582.
[17] T. Tanaka, S. Tohyama, M. Murata, F. Nomura, T. Kaneko, H. Chen, F. Hattori, T. Egashira, T. Seki, Y. Ohno, U. Koshimizu, S. Yuasa, S. Ogawa, S. Yamanaka, K. Yasuda, K. Fukuda, In vitro pharmacologic testing using human induced pluripotent stem cell-derived cardiomyocytes, Biochem. Biophys. Res. Commun. 385 (2009) 497–502.

Circ J 2009; **73:** 1397–1398

MicroRNA is a New Diagnostic and Therapeutic Target for Cardiovascular Disease and Regenerative Medicine

Ruri Kaneda; Keiichi Fukuda

MicroRNAs (miRNAs) are recently discovered regulatory RNA molecules consisting of 21 to 24 non-coding nucleotides that regulate gene expression by hybridizing to messenger RNAs (mRNAs) and causing mRNA degradation or translational inhibition[1] The importance of miRNAs has been demonstrated in model organisms, such as *Caenorhabditis elegans* and *Drosophila*, where they control key steps in development[2,3] However, recent evidence suggests that miRNAs participate in the control of heart development[4] the pathogenesis of cardiovascular disease[5,6,7] and the differentiation of embryonic stem cells into cardiomyocytes[8,9]

Article p 1492

MiRNAs are processed from precursor molecules (pri-miRNAs), which are either transcribed from independent miRNA genes or are portions of introns of protein-coding RNA polymerase II transcripts. A single pri-miRNA often contains sequences for several different miRNAs. Pri-miRNAs fold into hairpin structures containing imperfectly base-paired stems and are processed in 2 steps, catalyzed by the RNase III type endonucleases, Drosha and Dicer. Both Drosha and Dicer function in complexes with proteins containing dsRNA-binding domains (dsRBDs). The Drosha partner is DiGeorge syndrome critical region gene 8 (DGCR8) in mammals. The Drosha-DGCR8 complex processes pri-miRNAs into ~70-nucleotide hairpin structures known as pre-miRNAs. Some spliced-out introns correspond precisely to pre-miRNAs (mirtrons), thus circumventing the requirement for Drosha-DGCR8. In animals, pre-miRNAs are transported to the cytoplasm by exportin5, where they are cleaved by Dicer [complexed with TAR RNA binding protein (TRBP) in mammals] to yield ~20-bp miRNA duplexes. One strand is then selected to function as a mature miRNA, whereas the other strand is degraded. Occasionally, both arms of the pre-miRNA hairpin give rise to mature miRNAs. Following their processing, miRNAs are assembled into ribonucleoprotein (RNP) complexes called micro-RNPs (miRNPs) or miRNA-induced silencing complexes (miRISCs). The key components of miRNPs are proteins of the Argonaute (AGO) family[10]

The miRISCs help mediate miRNA:mRNA interactions according to a set of rules. One rule for miRNA-target base pairing is perfect and contiguous base pairing of miRNA nucleotides 2 to 8, representing the 'seed region', which nucleates the miRNA-mRNA association. GU pairs or mismatches and bulges in the seed region greatly affect repression. However, an A residue across position 1 of the miRNA, and an A or U across position 9, improve the site efficiency, although they do not need to base pair with miRNA nucleotides. Another rule is that there must be reasonable complementarity to the miRNA 3' half to stabilize the interaction. Mismatches and bulges are generally tolerated in this region, although good base pairing, particularly to residues 13–16 of the miRNA, becomes important when matching in the seed region is suboptimal[10] When miRISCs bind to mRNAs, they can repress their expression by several mechanisms: inhibition of translation elongation, co-translational protein

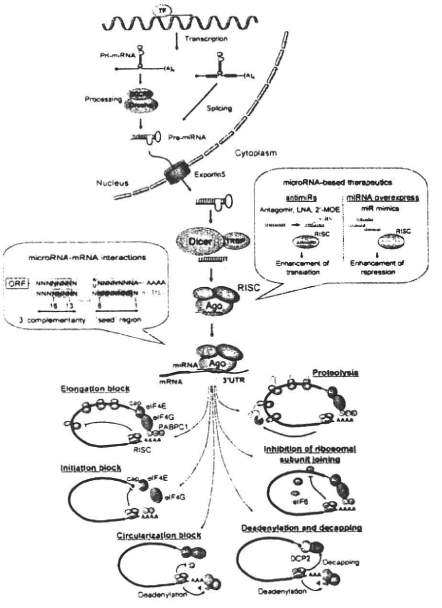

Figure. Schematic representation of micro RNAs (miRNA) processing and regulation. Transcription of miRNA genes (pri-miRNA) is mediated by RNA polymerase II. Pri-miRNAs are catalyzed by the RNase III type endonucleases, Drosha and Dicer. Mature miRNAs are assembled into miRNA-induced silencing complexes (miRISC). The miRISC helps mediate miRNA–mRNA interactions. MiRNA-target base pairing in 'seed regions' as well as 3' complementarity can affect their repression. When miRISC bind to mRNAs, they can repress their expression by several mechanisms: inhibition of translation elongation, proteolysis, competition for the cap structure, inhibition of ribosomal subunit joining, inhibition of mRNA circularization, deadenylation, and decapping. Anti-miRs (antagomir, LNA and 2'-MOE) enhance translation of the target gene. Conversely, miRNA mimics enhance the repression of the target gene.

(Received June 15, 2009; accepted June 15, 2009)
Department of Regenerative Medicine and Advanced Cardiac Therapeutics, Keio University School of Medicine, Tokyo, Japan
Mailing address: Keiichi Fukuda, MD, Department of Regenerative Medicine and Advanced Cardiac Therapeutics, Keio University School of Medicine, 35 Shinanomachi, Shinjuku-ku, Tokyo 160-8582, Japan.
E-mail: kfukuda@sc.itc.keio.ac.jp

degradation, competition for the cap structure, inhibition of ribosomal subunit joining, and inhibition of mRNA circularization through deadenylation and decapping![11]

In the field of cardiovascular disease or cardiomyogenesis during development, the function of the miRNA-1 (miR-1) and miRNA-133 (miR-133) families, which are specifically expressed in both skeletal muscle and the heart, have been investigated intensively. The vertebrate genome contains 2 distinct loci for the miR-1 and miR-133 bicistronic clusters that give rise to identical mature miRNA sequences. Although miR-133a is expressed in the same bicistronic unit as miR-1-1 or miR-1-2, miR-133b is expressed as a separate gene transcript. During skeletal myogenesis and in the developing heart, their tissue-specific expression is largely controlled by myogenic transcriptional networks involving transcriptional regulators, such as myocyte enhancer factor 2 (MEF2), serum response factor (SRF), MyoD, and myocardin![12–14] In cardiac myocytes, SRF induces the expression of miR-133, which in turn inhibits SRF itself in a feedback regulatory loop that affects differentiation and promotes progenitor proliferation. In skeletal muscle progenitors, miR-133 enhances myoblast proliferation by targeting SRF, whereas miR-1 promotes myogenesis by targeting the HDAC4. HDAC4 acts as a transcriptional repressor of MEF2. Thus, miR-1 and miR-133 participate in key negative feedback regulatory loops controlling the proliferation and differentiation status of skeletal and cardiac muscle progenitors![5]

Targeted deletion of the muscle-specific miRNA, miR-1-2, revealed numerous functions in the heart, including regulation of cardiac morphogenesis, electrical conduction, and cell-cycle control, which are processes controlled by this miRNA targeting the genes encoding Hand2 and Irx5, as well as those regulating the cell-cycle, and tumor suppressors![5] MiR-1 and miR-133 also regulate hypertrophic responses in the heart![6]

Takaya et al investigated the role of miR-1 and miR-133 during spontaneous myocardial differentiation of ES cells by 2-dimensional culture![9] The levels of miR-1 and miR-133 were increased during spontaneous differentiation but reduced during forced myocardial differentiation by the HDAC inhibitor, trichostatin A. The overexpression of miR-1 in ES cells by lentiviral infection reduces cardiomyogenesis via post-transcriptional inhibition of cyclin-dependent kinase-9 (Cdk9). In contrast, Ivey et al[8] reported that miR-1 promotes myocardial differentiation during the embryoid body-based culture of mouse and human ES cells by targeting the Notch ligand Delta-like1. Thus, muscle-specific miRNAs precisely regulate the spatiotemporal expression of target genes in different situations including myocardial differentiation, cardiovascular development, and adult cardiac disease.

Although the understanding of miRNA function is rapidly increasing, many challenges remain to utilize modulation of miRNA levels as a novel therapeutic strategy. First, the establishment of methods to accurately and efficiently determine the miRNA targets is essential. Current bioinformatics approaches have provided useful information, but precise targets must be identified among the many predicted targets. The identification of specific target genes would further our understanding of the mechanisms underlying cardiovascular disease pathogenesis. Second, the function of low expressed miRNAs including novel ones or other types of non-coding RNAs, which could be identified by high-throughput sequencing, should be analyzed as well as those expressed at higher levels in the heart. Third, proteins such as HuR, an AU-rich-element binding protein, that interact with the 3' untranslated region (3'UTR) of mRNA molecules, should be explored as they might act as modifiers to alter the potential of miRNAs to repress gene expression under stress conditions![16]

Furthermore, RNA-interference-based technologies have potential as a therapeutic strategy. Modified antisense oligonucleotides targeting the mature miRNA sequence, miRNA inhibitors (anti-miRs), including cholesterol-conjugated 2'-O-methyl oligonucleotide (antagomir), locked-nucleic-acid-modified oligonucleotide (LNA), and 2'-O-methoxyethyl phosphorothioate (2'-MOE), can reduce the levels of pathogenic or aberrantly expressed miRNAs![17] Conversely, miRNA mimics can serve to elevate the levels of miRNAs![18,19] Aberrant miRNA expression might become a novel strategy for the treatment of cardiovascular disease.

References

1. Ambros V. microRNAs: Tiny regulators with great potential. *Cell* 2001; **107:** 823–826.
2. Lee RC, Feinbaum RL, Ambros V. The *C. elegans* heterochronic gene *lin*-4 encodes small RNAs with antisense complementarity to *lin*-14. *Cell* 1993; **75:** 843–854.
3. Wienholds E, Kloosterman WP, Miska E, Alvarez-Saavedra E, Berezikov E, de Bruijn E, et al. MicroRNA expression in zebrafish embryonic development. *Science* 2005; **309:** 310–311.
4. Zhao Y, Samal E, Srivastava D. Serum response factor regulates a muscle-specific microRNA that targets Hand2 during cardiogenesis. *Nature* 2005; **436:** 214–220.
5. Zhao Y, Ransom JF, Li A, Vedantham V, von Drehle M, Muth AN, et al. Dysregulation of cardiogenesis, cardiac conduction, and cell cycle in mice lacking miRNA-1-2. *Cell* 2007; **129:** 303–317.
6. Carè A, Catalucci D, Felicetti F, Bonci D, Addario A, Gallo P, et al. microRNA-133 controls cardiac hypertrophy. *Nat Med* 2007; **13:** 613–618.
7. van Rooij E, Sutherland LB, Liu N, Williams AH, McAnally J, Gerard RD, et al. A signature pattern of stress-responsive microRNAs that can evoke cardiac hypertrophy and heart failure. *Proc Natl Acad Sci USA* 2006; **103:** 18255–18260.
8. Ivey KN, Muth A, Arnold J, King FW, Yeh RF, Fish JE, et al. MicroRNA regulation of cell lineages in mouse and human embryonic stem cells. *Cell Stem Cell* 2008; **2:** 219–229.
9. Takaya T, Ono K, Kawamura T, Takanabe R, Kaichi S, Morimoto T, et al. MicroRNA-1 and microRNA-133 in spontaneous myocardial differentiation of mouse embryonic stem cells. *Circ J* 2009; **73:** 1492–1497.
10. Filipowicz W, Bhattacharyya SN, Sonenberg N. Mechanisms of post-transcriptional regulation by microRNAs: Are the answers in sight? *Nat Rev Genet* 2008; **9:** 102–114.
11. Eulalio A, Huntzinger E, Izaurralde E. Getting to the root of miRNA-mediated gene silencing. *Cell* 2008; **132:** 9–14.
12. Chen JF, Mandel EM, Thomson JM, Wu Q, Callis TE, Hammond SM, et al. The role of microRNA-1 and microRNA-133 in skeletal muscle proliferation and differentiation. *Nat Genet* 2006; **38:** 228–233.
13. Rao PK, Kumar RM, Farkhondeh M, Baskerville S, Lodish HF. Myogenic factors that regulate expression of muscle-specific microRNAs. *Proc Natl Acad Sci USA* 2006; **103:** 8721–8726.
14. Liu N, Williams AH, Kim Y, McAnally J, Bezprozvannaya S, Sutherland LB, et al. An intragenic MEF2-dependent enhancer directs muscle-specific expression of microRNAs 1 and 133. *Proc Natl Acad Sci USA* 2007; **104:** 20844–20849.
15. Fazi F, Nervi C. MicroRNA: Basic mechanisms and transcriptional regulatory networks for cell fate determination. *Cardiovasc Res* 2008; **79:** 553–561.
16. Bhattacharyya SN, Habermacher R, Martine U, Closs ET, Filipowics W. Relief of microRNA-mediated translational repression in human cells subjected to stress. *Cell* 2006; **125:** 1111–1124.
17. Krützfeldt J, Rajewsky N, Braich R, Rajeev KG, Tuschl T, Manoharan M, et al. Silencing of microRNAs in vivo with 'antagomirs'. *Nature* 2005; **438:** 685–689.
18. Martinez J, Patkaniowska A, Urlaub H, Lührmann R, Tuschl T. Single-stranded antisense siRNAs guide target RNA cleavage in RNAi. *Cell* 2002; **110:** 563–574.
19. Jackson AL, Burchard J, Leake D, Reynolds A, Schelter J, Guo J, et al. Position-specific chemical modification of siRNAs reduces "off-target" transcript silencing. *RNA* 2006; **12:** 1197–1205.

Metabolic Remodeling Induced by Mitochondrial Aldehyde Stress Stimulates Tolerance to Oxidative Stress in the Heart

Jin Endo,* Motoaki Sano,* Takaharu Katayama,* Takako Hishiki, Ken Shinmura, Shintaro Morizane, Tomohiro Matsuhashi, Yoshinori Katsumata, Yan Zhang, Hideyuki Ito, Yoshiko Nagahata, Satori Marchitti, Kiyomi Nishimaki, Alexander Martin Wolf, Hiroki Nakanishi, Fumiyuki Hattori, Vasilis Vasiliou, Takeshi Adachi, Ikuroh Ohsawa, Ryo Taguchi, Yoshio Hirabayashi, Shigeo Ohta, Makoto Suematsu, Satoshi Ogawa, Keiichi Fukuda

Rationale: Aldehyde accumulation is regarded as a pathognomonic feature of oxidative stress–associated cardiovascular disease.

Objective: We investigated how the heart compensates for the accelerated accumulation of aldehydes.

Methods and Results: Aldehyde dehydrogenase 2 (ALDH2) has a major role in aldehyde detoxification in the mitochondria, a major source of aldehydes. Transgenic (Tg) mice carrying an *Aldh2* gene with a single nucleotide polymorphism (*Aldh2*2*) were developed. This polymorphism has a dominant-negative effect and the Tg mice exhibited impaired ALDH activity against a broad range of aldehydes. Despite a shift toward the oxidative state in mitochondrial matrices, *Aldh2*2* Tg hearts displayed normal left ventricular function by echocardiography and, because of metabolic remodeling, an unexpected tolerance to oxidative stress induced by ischemia/reperfusion injury. Mitochondrial aldehyde stress stimulated eukaryotic translation initiation factor 2α phosphorylation. Subsequent translational and transcriptional activation of activating transcription factor-4 promoted the expression of enzymes involved in amino acid biosynthesis and transport, ultimately providing precursor amino acids for glutathione biosynthesis. Intracellular glutathione levels were increased 1.37-fold in *Aldh2*2* Tg hearts compared with wild-type controls. Heterozygous knockout of *Atf4* blunted the increase in intracellular glutathione levels in *Aldh2*2* Tg hearts, thereby attenuating the oxidative stress–resistant phenotype. Furthermore, glycolysis and NADPH generation via the pentose phosphate pathway were activated in *Aldh2*2* Tg hearts. (NADPH is required for the recycling of oxidized glutathione.)

Conclusions: The findings of the present study indicate that mitochondrial aldehyde stress in the heart induces metabolic remodeling, leading to activation of the glutathione–redox cycle, which confers resistance against acute oxidative stress induced by ischemia/reperfusion. (*Circ Res.* 2009;105:1118-1127.)

Key Words: cardiac metabolism ■ oxidative stress ■ aldehyde ■ stress response

Aldehydes are the major end products of lipid peroxidation. They are highly electrophilic and react with biomolecules, such as proteins and nucleic acids, to generate various adducts.[1] Increased levels of aldehyde adducts have been detected in oxidized lipoproteins, atherosclerotic lesions, hearts with coronary artery disease, and Alzheimer brains.[2–4] In addition to the pathogenic effect associated with oxidative stress, sublethal levels of aldehydes interact with signaling systems to upregulate gene expression to counteract stressor challenges and to reestablish homeostasis.[5–7]

In mammalian cells, reactive aldehydes are detoxified by oxidation to carboxylates, a reaction catalyzed by aldehyde dehydrogenases (ALDHs).[1] The ALDHs are a superfamily of $NAD(P)^+$-dependent enzymes,[8] and, to date, 19 distinct *ALDH* genes have been identified in the human genome.[9] ALDH2 is localized to the mitochondria, a major source of

Original received June 19, 2009; resubmission received August 3, 2009; revised resubmission received September 25, 2009; accepted September 29, 2009

From the Department of Regenerative Medicine and Advanced Cardiac Therapeutics (J.E., M. Sano, T.K., S. Morizane, T.M., Y.K., Y.Z., H.I., F.H., K.F.); Cardiology Division (J.E., T.K., T.M., Y.K., S. Ogawa), Department of Internal Medicine; Department of Biochemistry and Integrative Medical Biology (T.H., Y.N., T.A., M. Suematsu); and Division of Geriatric Medicine (K.S.), Keio University School of Medicine, Tokyo, Japan; Precursory Research for Embryonic Science and Technology (PRESTO) (M. Sano), Japan Science and Technology Agency, Saitama, Japan; Department of Biochemistry and Cell Biology (K.N., A.M.W., I.O., S. Ohta), Institute of Development and Aging Sciences, Graduate School of Medicine, Nippon Medical School, Kawasaki, Japan; Department of Pharmaceutical Sciences (S. Marchitti, V.V.), University of Colorado Health Sciences Center, Denver; Department of Metabolome (H.N., R.T.), University of Tokyo, Japan; and Neuronal Circuit Mechanisms Research Group (Y.H.), Brain Science Institute, RIKEN, Saitama, Japan.

*Authors contributed equally to this work.

Correspondence to Dr Motoaki Sano, Department of Regenerative Medicine and Advanced Cardiac Therapeutics, Keio University School of Medicine, 35 Shinanomachi Shinjuku-ku, Tokyo, 160-8582, Japan. E-mail msano@sc.itc.keio.ac.jp

Circulation Research is available at http://circres.ahajournals.org

DOI: 10.1161/CIRCRESAHA.109.206607

reactive oxygen species and a target of membrane lipid peroxidation. ALDH2 has been implicated in cellular antioxidant processes because ALDH2 deficiency increases oxidative stress.[10,11] Furthermore, the cardioprotective effects of moderate alcohol consumption are well documented in animal models and humans,[12] and ethanol exposure, followed by sufficient time to metabolize the alcohol before ischemia, induces a delayed form of preconditioning-like cardioprotection.[13] The mitochondrial translocation of protein kinase Cε and the subsequent activation of ALDH2 have been shown to contribute to the cardioprotective effects of alcohol.[14] Indeed, administration of a small-molecule activator of ALDH2 to rats before an ischemic event reduced infarct size by 60%.[15]

A single nucleotide polymorphism of *ALDH2* (*ALDH2*2*), acts as a dominant-negative gene and is found in Asian populations (Figure I in the Online Data Supplement, available at http://circres.ahajournals.org). ALDH2 acts as a homo- or heterotetramer, and all tetramers that contain at least 1 ALDH2*2 subunit are inactive.[16] People homozygous for the ALDH2*2 allele (≈8% of the Japanese population) do not have any ALDH2 activity, whereas activity in individuals heterozygous for the ALDH2*2 allele (≈40% of the Japanese population) is as low as 1 in 16 of that in ALDH2*1 (wild-type [Wt]) homozygous individuals.[17] Notably, the Aldh2*2 allele has been reported to affect the metabolism of acetaldehyde, as well as other aldehydes, such as benzaldehyde (a metabolite of toluene) and chloroacetaldehyde (generated during the metabolism of vinyl chloride). The ALDH2*2 allele is associated with alcohol flushing syndrome, increased serum lipid peroxide levels,[18] and an increased risk for late-onset Alzheimer's disease.[19] Previously, we demonstrated that in stable transfectants of the PC12 neuronal cell line expressing mouse Aldh2*2, mitochondrial, but not cytosolic, Aldh activity was repressed.[10,11] The resultant Aldh-deficient transfectants were highly vulnerable to oxidative insult by exogenous 4-hydroxy-2-nonenal (4-HNE) or antimycin A. Furthermore, transgenic (Tg) mice expressing Aldh2*2 in their brains exhibited decreased ability to detoxify 4-HNE in cortical neurons and an accelerated accumulation of 4-HNE in the brain. Consequently, age-associated neurodegeneration accompanied by memory loss appeared in these mice after 1 year of age.[20] This phenotype mimics late-onset Alzheimer's disease in human.

In this study, we developed a Tg loss-of-function model for aldehyde-detoxifying enzymes to exploit the overexpression of Aldh2*2 in the heart, which simulates heterozygotes for the *ALDH2*2* allele in individuals already expressing Wt *ALDH2*1* in the heart. Despite a significant accumulation of 4-HNE adduct proteins in the mitochondrial matrices, left ventricular systolic and diastolic function were equivalent to that in Wt littermates until at least 2 years of age. Furthermore, the hearts exhibited enhanced tolerance to ischemia/reperfusion (I/R) injury. This is markedly different to the *Aldh2*2* Tg brain, where accumulation of 4-HNE in the brain was accompanied by neuronal cell death, indicating that the heart has a superior ability to resist mitochondrial aldehyde stress than the brain and exploits the hormesis-like effect of aldehydes. Thus, we subsequently investigated the molecular basis underlying this aldehyde-induced, hormesis-like stress response in *Aldh2*2* Tg hearts.

Non-standard Abbreviations and Acronyms

ALDH	aldehyde dehydrogenase 2
ATF4	activating transcription factor-4
eIF2α	α-subunit of eukaryotic translation initiation factor 2
Gcl	glutamate cysteine ligase
GSH	glutathione
GSSG	glutathione disulfide
GST	glutathione *S*-transferase
4-HNE	4-hydroxy-2-nonenal
I/R	ischemia/reperfusion
PHGDH	3-phosphoglycerate dehydrogenase
SLC	solute carrier
Tg	transgenic
Wt	wild type

Methods

*Aldh2*2* Tg mice were generated by pronuclear injection of a plasmid carrying *Aldh2*2* with a single nucleotide mutation at the same locus as the human *Aldh2*2* polymorphism. The mice used for these experiments were more than 10 generations back-crossed to C57BL/6 mice. For fluxome analysis, hearts were perfused with a modified Krebs–Henseleit buffer (120 mmol/L NaCl, 25 mmol/L $NaHCO_3$, 5.9 mmol/L KCl, 1.2 mmol/L $MgSO_4$, 1.75 mmol/L $CaCl_2$, 10 mmol/L glucose, 10 μU/mL insulin, 0.4 mmol/L oleate, and 1% BSA) gassed with 95% O_2/5% CO_2 at 37°C, according to the Langendorff procedure. After equilibration, the buffer was switched to modified Krebs–Henseleit buffer containing 10 mmol/L ^{13}C-glucose instead of 10 mmol/L glucose.

An expanded Methods section is available in the Online Data Supplement at http://circres.ahajournals.org.

Results

*Aldh2*2* Tg Mice Represent a Loss-of-Function Model of Aldh Activity

We created a loss-of-function model for aldehyde-detoxifying enzymes by Tg expression of *Aldh2*2* under control of the CAG promoter (Figure 1A). Strong expression of the Aldh2*2 protein was observed in the heart and skeletal muscles (Figure 1B). During development to reproductive maturity, *Aldh2*2* Tg mice exhibited small body size (Figure 1C and 1D), reduced muscle mass, diminished fat content (Figure 1E), osteopenia, and kyphosis. These phenotypes are not observed in *Aldh2*-null mice (ie, mice in which normal Aldh2 activity is blocked by knockout of the *Aldh2* gene).[21] These data indicate that the phenotypes observed in *Aldh2*2* Tg mice are not attributable simply to a lack of Aldh2 activity. We suspect that Aldh2*2 inactivates not only Aldh2, but also other Aldh subfamilies, presumably by forming heterotetramers.[22,23] Consistent with this, the forced expression of Aldh2*2 impaired Aldh activity against aliphatic aldehydes, including 4-HNE, whereas genomic disruption of *Aldh2* did not (Online Table I).

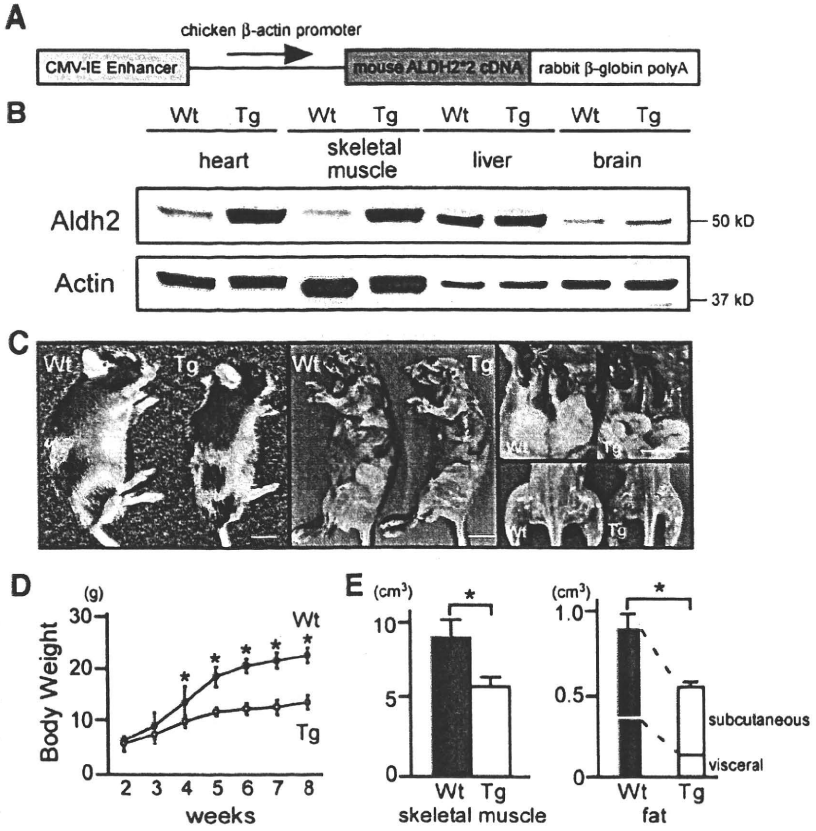

Figure 1. Characterization of *Aldh2**2* Tg mice. A, Design of the targeting construct. Recombinant murine Aldh2 (Glu487Lys) is expressed under the control of the CAG promoter. B, Tissue-specific expression of the *Aldh2**2* transgene. C, Senescence-like phenotypes of *Aldh2**2* Tg mice. Bars=1 cm. D, Growth curves of mice fed normal chow. E, Computed tomographic quantification of the composition of muscle and fat. Data are the means±SEM (n=6 to 8). *$P<0.05$ (unpaired Student's t test).

Mitochondrial Oxidative Stress in Aldh2*2 Tg Hearts

A cell fractionation study revealed that the Aldh2*2 protein is localized in the mitochondria (levels 8-fold higher than those of endogenous Aldh2; Figure 2A). Consistent with this, we found that levels of some 4-HNE adduct proteins were increased in the mitochondrial fraction of *Aldh2**2* Tg hearts. However, there was little increase in 4-HNE adduct protein levels in the cytosolic fraction of *Aldh2**2* Tg hearts.

The hearts of *Aldh2**2* Tg mice were smaller (in proportion to body size) than those of their Wt littermates (Figure 2B; Online Figure II, A). Light microscopic examination of *Aldh2**2* Tg hearts revealed normal alignment of thinner cardiomyocytes. Furthermore, there was no evidence of interstitial fibrosis or cellular degeneration/death (Figure 2C; Online Figure II, C). Ultrastructural analysis by transmission electron microscopy revealed that the sarcomere structure of the myofibrils in *Aldh2**2* Tg hearts was intact. Of note, some mitochondria contained electron-dense deposits on a few cristae (Figure 2D). Finally, a decline of mitochondrial function (Figure 3A) and a shift toward the oxidative state were found in mitochondrial matrices of *Aldh2**2*-expressing cells (Figure 3B).

*Aldh2**2* Tg Hearts Exhibit Greater Tolerance to Oxidative Stress

Echocardiographic examination of 3-month-old *Aldh2**2* Tg mice revealed normal left ventricular systolic and diastolic function (Online Figure III), indicating adaptation of the heart to persistent mitochondrial oxidative stress, at least under unstressed conditions.

To determine whether *Aldh2**2* Tg hearts are susceptible or resistant to exogenous oxidative stress elicited by I/R injury, isolated hearts were subjected to 30 minutes total global ischemia, followed by 60 minutes aerobic reperfusion. Notably, *Aldh2**2* Tg hearts exhibited significantly improved recovery of left ventricular developed pressure and ±dP/dt during reperfusion compared with the control group (n=6; $P<0.05$; Figure 4A and 4B). Consistent with these findings, total lactate dehydrogenase release into the perfusate during reperfusion was significantly lower in *Aldh2**2* Tg compared with control hearts (n=6; $P<0.05$; Figure 4C). In addition, we confirmed improved handling of I/R injury in in vivo hearts. Reperfusion injury was reduced in hearts from *Aldh2**2* Tg mice, as reflected by a reduction in the size of the necrotic zone per area at risk (n=6; $P<0.05$; Figure 4D).

Induction of Genes in Aldh2*2 Tg Hearts

Gene chip analysis revealed that the expression of genes for the major antioxidant enzymes was not induced in *Aldh2**2* Tg hearts, with the exception of the expression of the glutathione (GSH) *S*-transferase-a1 and -a2 (*Gsta1* and *Gsta2*) genes (Online Figure IV). Furthermore, there was no change in the expression of genes involved in the production of lipid mediators and reactive oxygen species, including *Xdh* and components of NADPH oxidase, in *Aldh2**2* Tg hearts (data not shown).

We found significant upregulation of genes encoding enzymes involved in amino acid biosynthesis and transport in

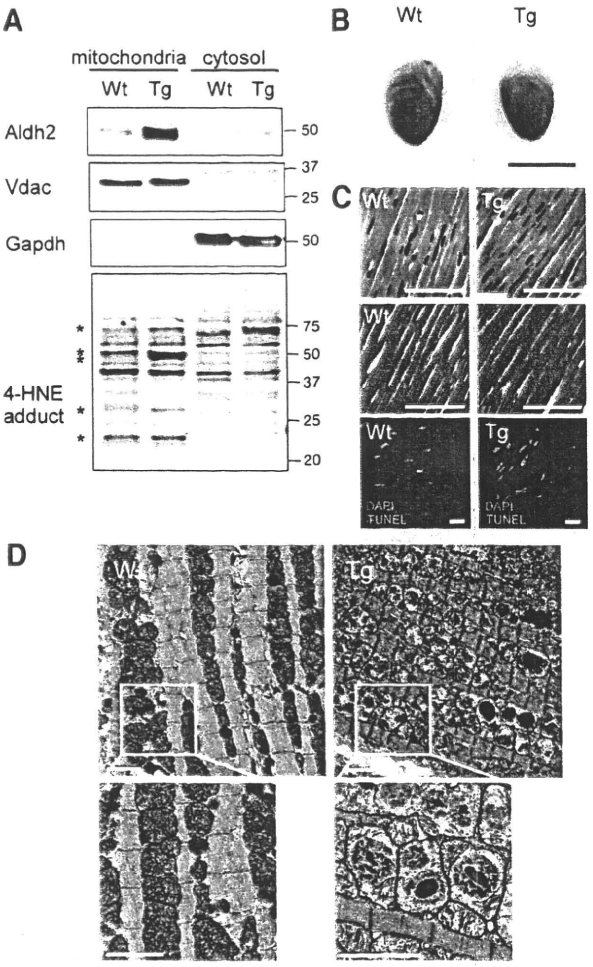

Figure 2. Characterization of hearts from *Aldh2*2* Tg mice. A, 4-HNE adduct proteins were determined in both mitochondrial and cytosolic fractions using Western blot analysis. Membranes were stripped and reprobed with ALDH2, VDAC (mitochondrial protein), and GAPDH (cytosolic protein). *Note that the intensity of 2 bands around 50 kDa, a band around 70, 30, and 23 kDa was stronger in the mitochondrial fraction for *Aldh2*2* Tg hearts vs Wt controls. B, Gross morphology of hearts. C, Microscopic analyses of hearts: hematoxylin/eosin staining (top images), Azan (middle images), and TUNEL (bottom images). Bars=100 μm. D, Ultrastructural analysis by transmission electron microscopy. Bars=2 μm.

*Aldh2*2* Tg hearts (Figure 5A), including genes encoding 3-phosphoglycerate dehydrogenase (*Phgdh*), phosphoserine aminotransferase 1 (*Psat1*), and phosphoserine phosphatase (*Psph*), all of which are involved in the 3-step conversion of 3-phosphoglycerate (a glycolytic intermetabolite) to serine. Serine hydroxymethyltransferase 1/2 (*Shmt1/2*) catalyzes the conversion of serine and tetrahydrofolate (THF) to glycine and 5,10-methylene THF, and methylenetetrahydrofolate dehydrogenase 2 catalyzes the interconversion of 5,10-methylene THF and 10-formyl THF. Cystathionase (*Cth*) is involved in cysteine biosynthesis in the *trans*-sulfuration pathway. These metabolic pathways eventually converge on GSH biosynthesis (for a metabolic map, see Figure 5B). Accordingly, despite the significant oxidative stress in the mitochondrial matrix, the intracellular concentration of GSH was increased 1.37-fold in *Aldh2*2* Tg compared with Wt hearts (n=8; $P<0.05$; Figure 6A). The synthesis of GSH from its constituent amino acids, namely L-glutamate, L-cysteine, and L-glycine, involves 2 enzymatic steps catalyzed by γ-glutamyl-cysteine ligase (Gclm, Gclc) and GSH synthetase (Gss).[24] However, induction of GSH biosynthetic enzymes was not particularly evident in *Aldh2*2* Tg hearts (Figure 5 and Online Figure V). The solute carrier (SLC) family of amino acid transporters, including members involved in cysteine biosynthesis or transport (*Slc1A4*, *Slc3A2*), was also upregulated in *Aldh2*2* Tg hearts. Notably, transcripts for the ATF/CREB (cyclic AMP response element–binding protein) (*Atf4*, *Atf5*) families of transcription factors, master regulators of amino acid metabolism,[25–28] were increased in *Aldh2*2* Tg hearts.

Glucose Biotransformation Is Shifted Toward the Pentose Phosphate Pathway

To further delineate changes in cardiac metabolism, intracellular concentrations of metabolites were measured by high-throughput metabolomics using capillary electrophoresis–mass spectrometry (CE-MS). The *Aldh2*2* Tg hearts exhibited characteristic changes in levels of metabolic intermediates of the glycolysis pathway (Online Figure VI). Specifically, levels of upstream glycolytic metabolites tended to increase, whereas those of downstream glycolytic metabolites tended to decrease in *Aldh2*2* Tg hearts. Notably, *Aldh2*2* Tg hearts contained higher levels of intermediate metabolites of the pentose phosphate pathway, including 6-phosphogluconate (1.42-fold increase) and ribose 5-phosphate (1.57-fold increase; n=6; $P<0.05$ vs Wt littermates). The myocardial NADPH/NADP$^+$ ratio was elevated in *Aldh2*2* Tg mice (n=6; $P<0.05$ versus Wt littermates; Figure 6B through 6D). There were no differences in glycogen content between Wt and *Aldh2*2* Tg hearts (0.016±0.002 and 0.018±0.003 μg/mg tissue, respectively).

Consistent with the upregulation of genes involved in amino acid metabolism and GSH biosynthesis, intracellular levels of glycine, homocysteine, and cystathionine were significantly higher in *Aldh2*2* Tg than Wt hearts (n=6; $P<0.05$; Figure 6E through 6G).

To verify the changes in glucose metabolism, we performed in vivo pulse-chase analysis of ^{13}C-labeled glucose (fluxome analysis) in Langendorff-perfused hearts (Figure 7). ^{13}C-Labeled metabolites were quantified by CE-MS 5 and 20 minutes after administration of ^{13}C-labeled glucose. ^{13}C-Labeled intermediate metabolites of the glycolytic and pentose phosphate pathways were higher in *Aldh2*2* Tg versus Wt hearts at both time points (n=6; $P<0.05$).

Phgdh, a rate-limiting enzyme for serine biosynthesis from intermediate metabolites of the glycolytic pathway (3-phosphoglycerate), was highly induced in *Aldh2*2* Tg hearts (Figure 8A). Accordingly, ^{13}C-labeled serine was markedly induced in ex vivo (Langendorff-perfused) and in vivo hearts (Online Figure VII).

To examine whether glucose uptake is actually augmented in *Aldh2*2* Tg hearts, Langendorff-perfused hearts were incubated with 2-deoxy-D-glucose (2-DG) for 5 minutes. When 2-DG is taken up into cells by glucose transporters, it

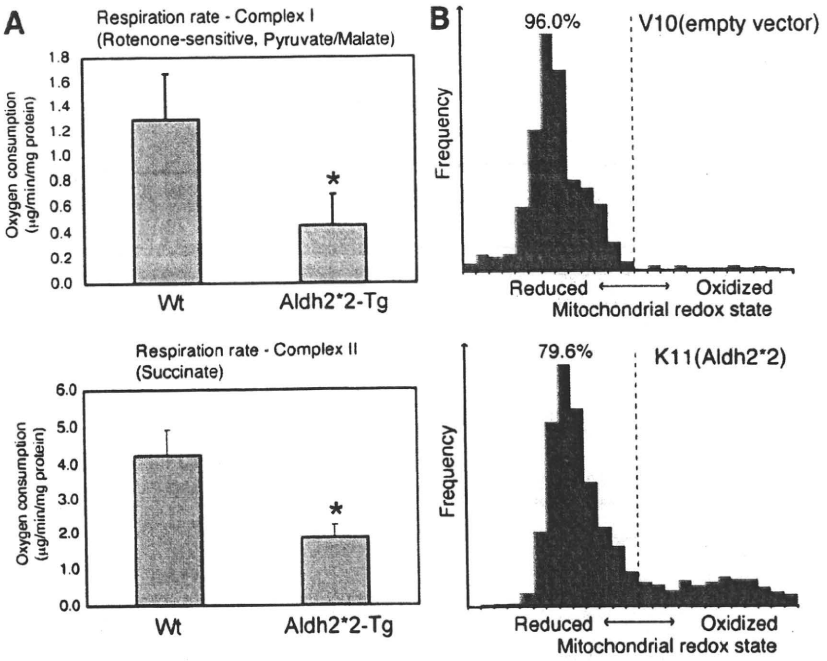

Figure 3. Characterization of *Aldh2**2*-expressing mitochondria. A, Comparison of oxygen consumption through complex I (top) and complex II (bottom) in mitochondria isolated from *Aldh2**2* Tg and Wt mice. Data are the means±SEM (n=5). **P*<0.05 vs Wt control (unpaired Student's *t* test). B, Comparison of redox status at the mitochondrial matrix between control (V10) and Aldh2*2 transfectants (K11). The mitochondrial redox state vs frequency is shown by histograms. The dashed line indicates 50% of roGFP1 oxidized/reduced. The percentage shows the relative number of cells with a >50% reduction in matrix.

is phosphorylated to 2-deoxy-d-glucose-6-phosphate (2-DGP). Because it cannot undergo further glycolysis, 2-DGP can be used as a measure of glucose uptake. As expected, intramyocardial accumulation of 2-DGP was 1.69-fold higher in *Aldh2**2* Tg compared with Wt hearts (n=6; $P<0.05$).

ATF4 Is a Key Transcriptional Regulator in Response to Aldehydes in the Heart

It is known that phosphorylation of the α subunit of eukaryotic translation initiation factor 2 (eIF2α) and subsequent translational activation of ATF4 result in the induction of additional members of the ATF/CREB family of transcription factors, which, together, upregulate a coordinately expressed set of genes involved in amino acid biosynthesis in mammalian cells.[25–28] Consistent with this, Western blot analysis demonstrated increased Ser51 phosphorylation on eIF2α and increased protein expression of Atf4 and Phgdh (Figure 8A) in *Aldh2**2* Tg versus Wt hearts.

To clarify the role of Atf4 in aldehyde-induced activation of amino acid metabolism and resistance to oxidative stress, *Aldh2* Tg mice were mated with Atf4-knockout mice.[29] Homozygous Atf4 knockout was lethal, whereas Atf4 heterozygous knockout ($Atf4^{+/-}$) mice, having half the Wt levels of Atf4 expression (Figure 8B), were viable with no cardiac anomalies under unstressed conditions. The increased expression of cardiac genes involved in amino acid metabolism in *Aldh2* Tg mice was significantly attenuated in *Aldh2* Tg mice carrying heterozygous alleles of *Atf4* (Figure 8C). Western blot analysis demonstrated that the increased levels of Phgdh protein in *Aldh2* Tg mice were reduced by half in *Aldh2* Tg mice carrying heterozygous alleles of *Atf4*. In addition, the increased intracellular GSH levels in *Aldh2* Tg

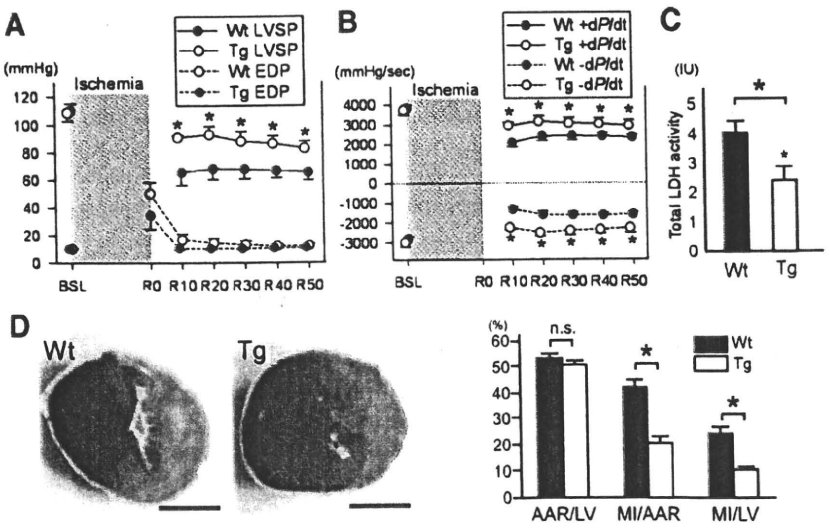

Figure 4. Function of the *Aldh2**2* Tg heart. Langendorff-perfused hearts were subjected to 30 minutes of total global ischemia, followed by aerobic reperfusion. A and B, Recovery of left ventricular systolic (LVSP) (A) and diastolic pressure (EDP) and ±dP/dt (B). C, Lactate dehydrogenase (LDH) release in the perfusate. D, Representative images of hearts from *Aldh2**2* Tg and Wt control mice after I/R injury (left). Quantification of infarct size (right). AAR indicates area at risk; BSL, baseline; LV, total left ventricular area; MI, area of myocardial infarction. **P*<0.05 vs Wt control (unpaired Student's *t* test).

A

symbol	Description	cy5_control1	cy3_Aldh2*2	ratio(cy5/cy3)
Atf4	activating transcription factor 4	372.7	1067.4	2.9
Atf5	activating transcription factor 5	175.4	1513.9	8.6
Phgdh	3-phosphoglycerate dehydrogenase	10.2	288.7	28.4
Psat1	phosphoserine aminotransferase 1	30.8	204.9	6.7
Psph	phosphoserine phosphatase	43.5	73.5	1.7
Shmt1	serine hydroxymethyl transferase 1 (soluble)	30.6	39.4	1.3
Shmt2	serine hydroxymethyl transferase 2 (mitochondrial)	207.8	270.4	1.3
Mthfd2	methylenetetrahydrofolate dehydrogenase (NAD+ depend	20.2	758.2	37.5
Gnmt	glycine N-methyltransferase	27.7	33.5	1.2
Cth	cystathionine gamma-lyase	28.3	38.6	1.4
Gclm	glutamate-cysteine ligase , modifier subunit	130.5	176.8	1.4
Gclc	glutamate-cysteine ligase, catalytic subunit	68.9	49.2	0.7
Gss	glutathione synthetase	60.0	59.3	1.0
Slc1a4	glutamate/neutral amino acid transporter	4.8	11.1	2.3
Slc7a11	Xc⁻ cysteine/glutamate transporter	6.3	6.5	1.0
Slc3a2	4F2 antigen heavy chain, amino acid transport	218.6	383.5	1.8
Slc7a3	cationic amino acid transporter, y+ system), member 3	3.8	31.8	8.3
Slc7a5	cationic amino acid transporter, y+ system), member 5	51.8	138.8	2.7
Gsta1	glutathione S-transferase, alpha 1 (Ya)	63.7	278.0	4.4
Gsta2	glutathione S-transferase, alpha 2 (Yc2)	29.3	176.1	6.0
Gsta3	glutathione S-transferase, alpha 3	95.7	95.5	1.0
Gsta4	glutathione S-transferase, alpha 4	1171.3	1408.3	1.2

Color codes: Global normalization intensity: > 100 > 20 > 5 > 2
Fold induction

B

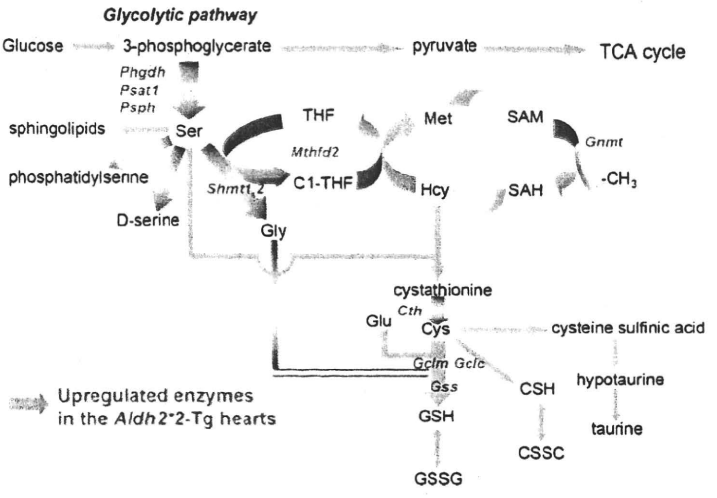

Figure 5. Transcriptome analysis of *Aldh2*2* Tg hearts. A, List of genes involved in amino acid metabolism that are upregulated in *Aldh2*2* Tg hearts (DNA Gene Chip analysis). B, Schematic representation of the serine biosynthetic pathway coupled with the *trans*-sulfuration pathway. SAH indicates *S*-adenosylhomocysteine.

mice were significantly attenuated in mice carrying the heterozygous alleles of *Atf4* (Figure 8D). Accordingly, heterozygous knockout of Atf4 attenuated the oxidative stress–resistant phenotype observed in *Aldh2*2* Tg hearts (Figure 8E).

Activation of ATF4 Is Crucial for the Oxidative Stress–Resistant Phenotype

Adenovirus-mediated expression of *Aldh2*2* in cultured cardiomyocytes increased immunoreactivity for 4-HNE adducts (Online Figure VIII, A), induced expression of *Atf4* and *Phgdh* (Online Figure VIII, B), and increased intracellular levels of reduced GSH (Online Figure VIII, C). The short interference (si)RNA-mediated knockdown of *Atf4* abolished the induction of *Phgdh* and the increase in intracellular GSH in *Aldh2*2*-expressing cardiomyocytes.

Consistent with the oxidative stress–tolerant phenotype observed for *Aldh2*2* Tg hearts, *Aldh2*2*-expressing cardiomyocytes exhibited enhanced tolerance to oxidative stress induced by glucose-free anoxia–reoxygenation or high-dose 4-HNE or antimycin A (Online Figure VIII, D; data not shown). The siRNA-mediated knockdown of Atf4 rendered the LacZ-expressing control cardiomyocytes vulnerable to oxidative stress and abrogated the oxidative stress–resistant phenotype of the Aldh2*2-expressing cardiomyocytes.

Discussion

The present study has demonstrated, for the first time, that the heart has an intrinsic capacity to change the metabolic pathways to counteract life-long mitochondrial oxidative damage. Mitochondrial aldehyde stress triggers phosphorylation of eIF2α and the combined transcriptional and translational activation of Atf4 upregulates the gene expression of enzymes involved in amino acid biosynthesis and transport that ultimately provide precursor amino acids for GSH biosynthesis, thereby increasing intracellular GSH levels. Surprisingly, hearts with chronic mitochondrial aldehyde stress exhibited improved tolerance to I/R injury despite the presence of substantial mitochondrial oxidative damages. Heterozygous knockout of *Atf4* blunted the increase in intracellular GSH levels in mitochondrial Aldh–deficient